(2)

UNCLASSIFIED
SECURITY CLASSIFICATION OF THIS PAGE

REPORT DOCUMENTATION PAGE	Form Approved OMB No. 0704-0188

AD-A243 747

	1b. RESTRICTIVE MARKINGS
LE	3. DISTRIBUTION/AVAILABILITY OF REPORT This document has been approved for public release and sale; its distribution is unlimited.
R(S)	5. MONITORING ORGANIZATION REPORT NUMBER(S)
Technical Report #35, IBM RJ #8248 (75442)	
6a. NAME OF PERFORMING ORGANIZATION IBM Research Division Almaden Research Center	6b. OFFICE SYMBOL (If applicable)
6c. ADDRESS (City, State, and ZIP Code) 650 Harry Road San Jose, CA 95120-6099	7a. NAME OF MONITORING ORGANIZATION Office of Naval Research
	7b. ADDRESS (City, State, and ZIP Code) Chemistry Division Code 1113 Arlington, VA 22217
8a. NAME OF FUNDING/SPONSORING ORGANIZATION Office of Naval Research	8b. OFFICE SYMBOL (If applicable)
8c. ADDRESS (City, State, and ZIP Code) Chemistry Division, Code 1113 Arlington, VA 22217	9. PROCUREMENT INSTRUMENT IDENTIFICATION NUMBER N00014-91-C-0166, 4131022
	10. SOURCE OF FUNDING NUMBERS PROGRAM ELEMENT NO. / PROJECT NO. / TASK NO. / WORK UNIT ACCESSION NO.

11. TITLE (Include Security Classification)
Detection And Spectroscopy Of Single Pentacene Molecules In A p-terpheny Crystal By Means Of Fluorescence Excitation

12. PERSONAL AUTHOR(S)
W. P. Ambrose, Th. Basche, W. E. Moerner

13a. TYPE OF REPORT	13b. TIME COVERED	14. DATE OF REPORT (Year, Month, Day)	15. PAGE COUNT
Interim Technical	FROM _____ TO _____	July 22, 1991	50 pages

16 SUPPLEMENTARY NOTATION

17. COSATI CODES			18. SUBJECT TERMS (Continue on reverse if necessary and identify by block number)
FIELD	GROUP	SUB-GROUP	Single molecule spectroscopy Ultrasensitive detection Pentacene in p-terphenyl

19 ABSTRACT (Continue on reverse if necessary and identify by block number)

Recent advances in fluorescence excitation spectroscopy with high efficiency have produced greatly improved optical spectra for the first electronic transition of individual single molecules of pentacene in *p*-terphenyl crystals at low temperatures (1.5 to 10 K). Two classes of single molecule behavior are observed: class I molecules have time-independent resonance frequencies, and class II molecules show a diffusive motion among several resonant frequencies with time which we term "spectral diffusion" by analogy with a similar effect which is common in amorphous materials. The temperature dependence of the linewidth and the power dependence of the fluorescence emission rate and of the linewidth are reported and analyzed. Various forms of the surprising class II behavior are described, including jumping among several discrete frequencies, creeping toward the center of the inhomogeneous line in many small steps, and a wandering among many possible resonance frequencies. The occurrence of class II behavior is restricted to the wings of the inhomogeneous line suggesting that the effect is correlated with some form of local disorder. The spectral diffusion rate

91-18761

20. DISTRIBUTION/AVAILABILITY OF ABSTRACT	21. ABSTRACT SECURITY CLASSIFICATION
☒ UNCLASSIFIED/UNLIMITED ☐ SAME AS RPT ☐ DTIC USERS	UNCLASSIFIED
22a NAME OF RESPONSIBLE INDIVIDUAL Dr. W.E. Moerner	22b TELEPHONE (Include Area Code) (408) 927-2426 / 22c OFFICE SYMBOL

increases with increasing temperature, suggesting that the effect may be due to phonon-assisted transitions of local degrees of freedom around the pentacene defect whose source remains to be identified conclusively.

OFFICE OF NAVAL RESEARCH

Contract N00014-91-C-0166

R&T Code 4131022

Technical Report No. 35

Detection And Spectroscopy Of Singe Pentacene Molecules In A *p*-Terphenyl Crystal By Means Of Fluorescence Excitation

by

Th. Basche, W. P. Ambrose, and W. E. Moerner

Prepared for Publication

in

Proceedings of the Society of Photo-Optical Instrumentation Engineers

IBM Research Division
Almaden Research Center
650 Harry Road
San Jose, California 95120-6099

July 22, 1991

RJ 8248 (75442) July 22, 1991
Physics

DETECTION AND SPECTROSCOPY OF SINGLE PENTACENE MOLECULES IN A *P*-TERPHENYL CRYSTAL BY MEANS OF FLUORESCENCE *EXCITATION*

W. P. Ambrose , Th. Basché, and W. E. Moerner

IBM Research Division
Almaden Research Center
650 Harry Road
San Jose, California 95120-6099

ABSTRACT: Recent advances in fluorescence excitation spectroscopy with high efficiency have produced greatly improved optical spectra for the first electronic transition of individual single molecules of pentacene in *p*-terphenyl crystals at low temperatures (1.5 to 10 K). Two classes of single molecule behavior are observed: class I molecules have time-independent resonance frequencies, and class II molecules show a diffusive motion among several resonant frequencies with time which we term "spectral diffusion" by analogy with a similar effect which is common in amorphous materials. The temperature dependence of the linewidth and the power dependence of the fluorescence emission rate and of the linewidth are reported and analyzed. Various forms of the surprising class II behavior are described, including jumping among several discrete frequencies, creeping toward the center of the inhomogeneous line in many small steps, and a wandering among many possible resonance frequencies. The occurrence of class II behavior is restricted to the wings of the inhomogeneous line suggesting that the effect is correlated with some form of local disorder. The spectral diffusion rate increases with increasing temperature, suggesting that the effect may be due to phonon-assisted transitions of local degrees of freedom around the pentacene defect whose source remains to be identified conclusively.

I. Introduction and Background

Optical spectroscopy of single impurity centers in condensed matter represents a powerful new probe of truly local, microscopic environments and impurity-host interactions in condensed matter. Unlike the highly successful tunnelling and atomic force microscopies [1-3] where single atoms or molecules must be bound to a surface and detection is performed in the near field, optical single-center spectroscopy in solids can probe deep within a sample in a relatively non-invasive fashion. However, optical diffraction and the resulting far-field detection require special techniques for the localization of single centers. Another powerful single-center method, the optical spectroscopy of single ions confined in electromagnetic traps [4,5], has led to a variety of novel measurements that test our understanding of quantum physics. In this case, the surrounding vacuum presents essentially no background signal, whereas in condensed matter there is the possibility that Raman and Rayleigh scattering from the solid itself can obscure the signal from a single impurity center.

In liquids, a number of researchers have concentrated on the detection of single fluorescently labeled molecules for analytical applications without recording detailed spectra. By using laser-induced fluorescence and a novel hydrodynamically-focused flow to confine the molecules and reduce the scattering volume, single molecules of the protein B-phycoerythrin with the equivalent of 25 rhodamine 6G chromophores were detected [6,7]. This work has recently allowed detection of the presence of single molecules of rhodamine 6G using photon burst detection[8] and correlation techniques[9].

The analogous problem of detection and spectroscopy of a single impurity absorber in a solid (called in the case of a molecular absorber, single-molecule detection, or SMD) would provide a useful tool for the study of local host-absorber interactions where the absorbing

center is essentially at rest, confined by the host lattice, and where the normal averaging over many "equivalent" centers is removed. Although this paper focuses on molecular impurity centers, the physical concepts apply equally well to ions, color centers, and other defect absorptions in solids.

Compared to the other single-absorber experiments, SMD in solids provides a different set of experimental challenges. Except in the case of an extremely special solid sample in which only one defect center is present, a crucial issue for SMD in solids is the method of selection of one defect out of many other identical defects that may be in the probing volume. As is well-known, at liquid helium temperatures, absorbing impurity (guest) centers in solids with zero-phonon transitions form inhomogeneously broadened lines, [10] where the overall line profile is caused by a (usually Gaussian) distribution of center frequencies for the individual absorbers that is broader than the (usually Lorentzian) homogeneous lineshape of the individual absorbers. The distribution of center frequencies is caused by dislocations, point defects, or random internal electric and strain fields and field gradients in the host material. The ratio between the inhomogeneous width and the homogeneous width is largest at low temperatures, because the homogeneous zero-phonon lines become much narrower than the inhomogeneous distribution only when the host phonons are quenched. In this regime, a single defect can be selected for spectroscopy simply by selecting a laser probing frequency that is far out in the wings of the inhomogeneous line where only one defect is in resonance. By utilizing samples with smaller and smaller defect densities, single absorbers can also be studied at any arbitrary position relative to the inhomogeneous line center.

Before proceeding to the single-center limit, it was necessary to understand fully the properties of inhomogeneously broadened lines when the number of centers in resonance is much greater than unity. Inhomogeneously broadened absorption lines are finite sums of the discrete absorption profiles of individual defect centers, hence the optical absorption itself

should contain an intrinsic "bumpiness" as a function of wavelength (as long as spectral hole-burning or spectral diffusion are not strong) even when the number of absorbers per homogeneous width $\overline{N}_H$ is large. This effect has been termed "statistical fine structure" or SFS, and it was observed for the first time [11,12] using the well-studied [13, 14] model system pentacene in *p*-terphenyl. Central to these measurements was the use of a powerful zero-background laser technique called frequency-modulation spectroscopy (FMS), first described by Bjorklund[15] in 1980. SFS results from (static) number fluctuations in the spectral density of absorbers with optical wavelength, and therefore the rms value of the spectral variations scales as the square root of $\overline{N}_H$.

Subsequent to the first observations of SFS, other researchers moved closer to single-absorber detection in solids by observing SFS at increasingly smaller values of $\overline{N}_H$. Lange et al. [16] relied upon fluorescence excitation of Sm^{2+} ions in CaF_2 at 77K with a fixed frequency laser in tightly focused spots. These researchers saw Poisson fluctuations in the detected fluorescence as a function of the position of the focal spot and concluded that they had reached the level $\overline{N}_H = 5$. Another novel approach, developed by Yen[17], used laser fluorescence excitation in a glass fiber doped with Nd^{3+} ions. Here the fiber geometry effectively maintains a small focus and a small probing volume in order to reduce background signals from the host. The measured SFS led these researchers to conclude that they had reached $\overline{N}_H$ values on the order of a few tens of ions. In both cases, special detection geometries were necessary to avoid host background fluorescence.

With a firm understanding of SFS in inhomogeneous lines, it became possible to approach the ultimate limit of single center detection and spectroscopy, $\overline{N}_H \leq 1$. One reason for studying single absorbers rather than a large number of absorbers at the same frequency is the fact that for an inhomogeneously broadened line, the various centers located within a homogeneous width of a given laser frequency are located at that particular spectral position

for a variety of possible reasons in general. This intrinsic multi-dimensional inhomogeneity cannot be removed with spectral hole-burning or coherent transient techniques. However, with SMD the absorption spectrum of an individual absorber can become directly accessible, as long as no other centers are present at the same frequency. This is a primary reason to pursue the spectroscopy of individual centers in condensed matter. Other motivations come from the fact that a single molecular impurity is a truly local probe of the minute details of a single local environment in a solid.

The first optical spectra of a single impurity center in condensed matter were reported for the case of the pentacene molecule in a crystal of *p*-terphenyl [18-20]. This observation required the use of a complex double-modulation absorption technique, in order to avoid potential background problems with Rayleigh and Raman scattering and residual amplitude modulation. Although the reported spectra do represent the achievement of SMD, the signal-to-noise ratio (SNR) of only $\simeq$ 3-5 with some minutes of averaging coupled with laser intensities above the saturation level made new physical measurements on the observed single molecules difficult. The SNR in these experiments was limited by laser shot noise and a small amount of avalanche multiplication noise from the avalanche photodiode used for the measurement.

The pentacene in *p*-terphenyl system is well-suited for SMD, owing to the large peak absorption cross section at low temperatures and the near-absence of spectral hole-burning effects[11]. Recently, Orrit et al.[21] also utilized the pentacene in *p*-terphenyl system to demonstrate that an alternative to the absorption approach, fluorescence excitation with highly efficient collection of the emitted photons and very small probing volumes, can yield superior SNR for single-molecule spectroscopy. The technique consists of using extremely thin sublimed samples and a paraboloidal mirror with numerical aperture (N. A.) near unity

to efficiently collect the fluorescence. The primary significance of this work is the direct illustration that the problem of scattering backgrounds can be overcome.

Using similar techniques, we have observed two distinct classes of behavior for single molecules of pentacene in *p*-terphenyl, termed class I and class II, and the detailed spectroscopy, temperature, wavelength, and intensity dependence of these single absorbing centers forms the subject of this paper. A preliminary report of the results has appeared [22,23]. Class I pentacene defects (described in Section III.A) have optical absorption frequencies that do not change with time and Lorentzian lineshapes with the lifetime-limited width at 1.5 K at sufficiently low probing laser intensity. Class II defects (Section III.B) have similar lineshapes and widths; however, these centers in addition show a variety of fascinating spectral diffusion effects, i.e., the optical absorption of class II pentacene molecules diffuses in frequency space as a function of time. Both discontinuous jumps in resonance frequency as well as a quasi-continuous wandering in frequency space with time have been observed, and the rate of resonant frequency changes does not appear to depend upon probing laser power. The analysis and discussion of the results will be described in Section IV.

It is clear that a single molecule of pentacene in *p*-terphenyl is an exquisitely sensitive probe of the detailed local environment around the impurity molecule. It appears that in certain regions, the *p*-terphenyl crystal may contain two-level tunnelling systems not unlike those that are intrinsic to the amorphous state, or perhaps other local degrees of freedom of unknown character. Indeed, the spectral diffusion effects reported here would appear only as a broadening of the optical absorption for any spectroscopy that averages over the behavior of many defects. With these observations, a new regime of optical spectroscopy may be envisioned in which some of the scientific advances and observations of physical

effects made possible by the ion trap and STM techniques may be attempted in condensed matter.

II. Experimental

Due to the difficulty of these measurements and to allow researchers to duplicate our SMD apparatus, the experimental configuration will be described in some detail. Crystals of *p*-terphenyl doped with trace amounts of pentacene were grown by cosubliming the separate materials. The starting materials were purified by zone refining in the case of *p*-terphenyl and by sublimation of pentacene. For cosublimation at different rates, a sublimation apparatus was constructed which contained two chambers maintained at different temperatures by two oil baths. *p*-Terphenyl was routinely sublimed at 170 to 180°C, and pentacene was sublimed at temperatures from 90 to 150°C. The resulting *p*-terphenyl crystal platelets have elongated hexagonal shapes, which are less than 10 μm thick and up to 7 mm wide. Crystal thicknesses were determined by measuring optical interference fringe spacings in a room temperature uv-visible spectrometer.

Pentacene concentrations ranged from $\simeq 10^{-6}$ to 10^{-9} mole/mole . Qualitative amounts of pentacene were determined in the higher concentration samples by observing the amount of pink fluorescence emitted at room temperature under ultraviolet excitation. Concentrations of other crystal samples were determined by various optical methods. The concentration of a 3×10^{-6} mole/mole sample was determined from the integrated (0-0) $S_1 \leftarrow S_0$ polarized optical absorption spectrum at 1.5 K (peak transmittance = 0.94 under unpolarized light) and the published transition dipole moment of 0.71 $\pm$ 0.24 Debye[24]. The amount of pentacene in $\simeq 10^{-6}$ to 10^{-8} mole/mole samples was determined by the relative intensity of the fluorescence emission at 1.5 K excited in the $S_0 \rightarrow S_1$ transition in a 1 mm spot using the 3×10^{-6} mole/mole sample measured in absorption as reference. The lowest

concentration of 8×10^{-9} mole/mole was determined by counting 830 molecules in a $\simeq 200\,\mu m^3$ volume of crystal in the O_1 inhomogeneous line distribution as observed using low-temperature fluorescence excitation.

Figure 1 shows the sample assembly used for single molecule detection by fluorescence excitation spectroscopy. The sample and two optical elements are mounted on mechanical positioners, and the entire assembly is immersed in superfluid liquid helium or in cooled helium gas. The excitation laser beam enters the sample assembly from the left in the figure, is focused through the sample with a small laser-grade achromat lens, and is then absorbed by a piece of black tape. The sample is placed at the focus of an N.A. = 0.98 paraboloid (P) (Optical Radiation Corp.), which collects and collimates 42 % of the emission from the sample. The choice of material for the sample substrate is determined by the need for a low Raman scattering background -- the sample substrate is a single crystal of NaCl or other alkali halide, which has no first-order Raman scattering. Samples have been mounted with NaCl cover plates or by using wax paper tabs and tape to hold the edges in place. Care must be taken not to strain samples during the mounting procedure, which can greatly broaden the inhomogeneous line distribution.

Focusing of the laser beam into the sample is accomplished by bending a thin stainless steel sheet with an electromagnetic actuator consisting of a coil (C) and magnet (M). The lens displacement rate is $\simeq 0.5\,\mu m/mA$, and the typical operating current is less than 100 mA into the 1 Ω coil (at 1.5 K). To verify that the laser is focused in the sample, the back-reflected laser light is observed outside the cryostat. With a collimated input beam, light reflected from the sample back through the input lens is collimated when the focus is at a sample surface. In some cases, a 2 mm diameter aluminum dot has been evaporated on the NaCl substrate, which aids in locating the substrate surface during focusing. After focusing on the aluminum surface, the sample mount is translated to move the aluminum dot out of

the laser beam, and the laser is focused into the sample. Fine adjustment of the laser beam into the sample is then performed by maximizing either the SFS at the center of the inhomogeneous distribution, or the single molecules themselves far from the center of the inhomogeneous distribution.

The temperature dependence of single molecule linewidths and spectral diffusion processes was examined between 1.5 and 10 K. The sample temperature was measured with a calibrated carbon resistor mounted near the sample. For temperatures between 1.5 and 4.2 K, the sample was immersed in liquid He and the temperature was controlled by throttling the He gas pumping rate. Above 4.2 K, the sample temperature was controlled by warming the He gas before it entered the sample chamber. For some of the temperature dependent work, the laser focusing lens in Fig. 1 was replaced by a single-mode polarization-preserving optical fiber (York HB600), which was bonded to the sample by an optical couplant or an epoxy.

Figure 2 shows the optical arrangement for laser focal spot translation and frequency calibration. A single frequency rhodamine 6G dye laser (DL) (Coherent 599-21, $\simeq$1-2 MHz linewidth) beam passes through a Faraday rotation optical isolator (OI) and an amplitude stabilizer (LAS) before being split by a beam splitter (BS). The transmitted beam is used to calibrate the frequency scan range, and the beam reflected from the beam splitter is conditioned and directed into the sample assembly. The sample assembly shown in Fig. 1 is inserted into an optical immersion helium cryostat at the sample position (S) in Fig. 2.

In Fig. 2, a $LiTaO_3$ electro-optic modulator (EOM), confocal Fabry-Perot étalon (FP) with 1.5 GHz free-spectral-range, and a photodiode (PM) are used to calibrate the relative laser frequency during laser scans less than a few GHz wide. A precision radio frequency (rf) source is used to drive the EOM, which is operated at fixed frequencies between 30 and 200 MHz. The laser beam is phase modulated by the EOM producing as many as 8 narrow

sidebands spaced by multiplies of the rf driving frequency about the laser frequency. Tuning the laser frequency through a resonance of the FP étalon and observing the comb of sidebands with the photodiode produces an accurate relative frequency reference which is independent of the exact free-spectral-range of the étalon. The absolute (vacuum) frequency of the laser is measured to within 1 GHz with a wavemeter (not shown in the figure).

The unmodulated beam reflected from the beam splitter in Fig. 2 is used to excite fluorescence from pentacene molecules after a sequence of laser beam conditioning and steering optics. First, the laser power is attenuated by fixed and variable attenuators (VA). A 60 cm single mode polarization-preserving optical fiber is then used to spatially filter the laser beam (SF), which is needed for a TEM_{∞} Gaussian beam at the sample. The collimated beam emerging from the SF is repolarized (P), and the polarization direction is set with a Fresnel rhomb (FR).

Fine translation of the laser focal spot across the sample surface is accomplished by pivoting the laser beam about the center of the sample assembly lens (L) in Fig. 1. In Fig. 2, pivoting the angle of the laser beam about the sample lens is performed with the tilt-mirror (TM), a micrometer screw (M) at the end of a $R_M = 352$ mm long lever attached to the TM, a spherical mirror (SM) with an $R_{SM} = 80$ cm radius, and the $f_S = 10$mm focal length lens mounted on the sample assembly (S) (lens L in Fig. 1). The TM and sample lens are each a distance R_{SM} from the SM. With this arrangement, the laser beam pivots about the points TM and S in Fig. 2. It is convenient to have a collimated beam entering the sample lens, so a lens is placed before the TM to focus the laser beam at $R_{SM}/2$, which results in a collimated beam leaving the SM. For small pivot angles, the ratio of laser focal spot to micrometer displacements is $\Delta X_S/\Delta X_M = 2(f_S/R_M) = 1/17.6$. Thus, 10$\mu$m steps at the micrometer are levered down to 0.568 μm translations of the laser focal spot across the

sample face. The theoretical displacement ratio $\Delta X_S/\Delta X_M$ was checked by locating the edges of a 25 μm hole in a metal foil with the laser focused to 5 μm full width at half maximum.

The laser power at the sample is controlled by attenuators (A and VA), and is monitored by a photodiode-based power meter (PM). The laser power meter calibration was checked against a calibrated thermopile. The laser power at the sample was varied from approximately 10 pW to 5 μW for various experiments.

It is important to properly orient the laser polarization at the sample. The *p*-terphenyl crystal is monoclinic (low symmetry) and the four substitutional sites occupied by pentacene molecules are both oriented and have well separated optical frequencies. Further, the optical absorption of pentacene is polarized along the short axis of the molecule [25,26]. Empirically, we find that the O_1 site absorption is polarized and oriented near the long axis of our sublimed *p*-terphenyl platelets. The laser polarization at the sample is first aligned with the long axis of the platelet, and fine adjustment of the polarization orientation is then made while observing the statistical fine structure (SFS) in the O_1 site inhomogeneous distribution (centered at 592.321 nm), or while observing fluorescence excitation spectra of single pentacene molecules in O_1 sites in at 1.5 K.

Photons emitted from the sample and collimated by the paraboloid (see Fig. 1) are long-pass filtered (F2 in Fig.2) and detected by a cooled RCA C31034A-02 or Hamamatsu R943-02 GaAs photomultiplier tube (PMT). Photon counting electronics are used to record the detected photons. Unwanted photons from room lights are filtered with a combination of long and short wavelength interference filters (F1) to form a 550 to 650 nm entrance window. Rayleigh-scattered laser light from the sample and sample assembly at the laser wavelength (between 592.2 and 592.7 nm for these experiments) is attenuated with 630 nm long pass filters (F2 , two 3 mm Schott RG630). Pentacene fluorescence and *p*-terphenyl Raman scattered light are Stokes shifted to longer wavelengths (by excitation of molecular

vibrations), and pass through filter F2; the zero-phonon pentacene fluorescence is not collected. The *p*-terphenyl Raman scattered light is made much weaker than the pentacene fluorescence as a result of the small sample volume pumped by the laser light.

As a means of calibrating the emission rate from single pentacene molecules, an overall photon collection and detection efficiency D was computed. The N.A. = 0.98 paraboloid collects 0.42 of the total solid angle about the sample. Five windows, a lens, and the low pass filters have a transmittance of 0.20 to the total emitted fluorescence. Finally, the GaAs PMT has a quantum efficiency of 0.13. Hence, the overall collection and detection efficiency is $D = 0.42 \times 0.20 \times 0.13 = 0.011 \pm 0.001$.

The level of long-term drift in the laser frequency was examined by measuring sharp, stable saturation holes in I_2 vapor. Hyperfine-level saturation holes were burned into the zero velocity component of I_2 gas with counter-propagating frequency-modulated laser beams at 592.336 nm[27]. The laser drift was measured at 30 MHz/hour (0.5 MHz/min), which is within the manufacturer's specification of less than 100 MHz/hour (1.6 MHz/min). In experiments with long integration times where this drift is non-negligible (as in the low-power linewidth measurements), the laser drift is removed by recording multiple fast scans (typically a few seconds over several hundred MHz) with an Analogic DP6100 Waveform Processor, locating the center frequency of a single molecule's fluorescence excitation spectrum in each scan, and averaging the spectra together with the center frequencies aligned. These functions are performed automatically using a small program running in the DP6100. Similarly, for experiments in which jumps in the resonance frequency of a single molecule are desired, a DP6100 program finds the peak frequency and records successive values of this peak frequency as a trend.

III. Results

A. Spectroscopy of stable class I pentacene defects

Figure 3 shows fluorescence excitation spectra for a $\simeq 10\,\mu$m thick, low concentration sample of pentacene in *p*-terphenyl at 1.5 K. To acquire these data, the sample was excited with 2 nW of laser power in a $5\,\mu$m focal spot, and the laser was tuned over 18 GHz in a 10 min time interval. Long-wavelength fluorescence photons were collected and counted in 30 ms count intervals. Trace 3 (a) shows an 18 GHz spectrum covering the central part of the inhomogeneous distribution for the O_1 site at 592.321 nm. The large structures appearing to be noise near the center of the spectrum are not noise, but static statistical fine structure reported earlier (at far higher concentration) using FM absorption spectroscopy[11]. Traces 3 (b) are two separated spectra taken $\simeq$ 10 min apart showing the reproducibility of the structure near the center of the distribution. *This structure is static and arises directly from* statistical variations in the spectral density of absorbers with laser frequency, or, equivalently, from the discreteness of the individual molecular contributions to the overall absorption. More interesting are the spectral features in the wings of the inhomogeneous distribution shown in traces 3 (b). At a detuning of -2.7 GHz, clearly resolved, individual single-molecule peaks are observed. Similar single molecule peaks are present on the blue edge of the inhomogeneous distribution, and in the wings of the O_2 site inhomogeneous line. The heights of the single-molecule peaks vary since the molecules are excited at different rates within the Gaussian laser intensity profile.

The total pentacene concentration for the sample shown in Fig. 3 can be estimated directly by counting the number of molecules in the spectrum. By comparing the average area of one molecule in Fig. 3 to the total area, there are $\simeq$ 830 molecules in O_1 sites in the focal volume. Since pentacene molecules are equally distributed over 4 sites, the focal volume

contains 3300 pentacene molecules. Since the focal volume is $\simeq 200\,\mu m^3$, the total pentacene concentration is $1.7 \times 10^{13}/cm^3$ or 8×10^{-9}mole/mole.

Sublimation platelets receiving different amounts of mechanical strain during handling, sample mounting, and cooling to low temperatures have different inhomogeneous line widths. The 2 GHz wide inhomogeneous distribution in Fig. 3 is for a carefully prepared and mounted sublimation platelet, for which the inhomogeneous linewidth varied little from position to position on the sample (although the statistical fine structure and individual single molecule peaks do vary, as will be seen below). On subsequent handling and repeated thermal cycling of this sample, an inhomogeneous broadening of up to 10 GHz was observed, which varied from position to position on the sample. In other samples receiving more strain during sample mounting and cool-down, single pentacene molecules may be found as far as $\simeq$ 200 GHz from line center at 592.321 nm wavelength. (Only scattered background light and no pentacene molecules are observed beyond $\simeq$592.7 nm wavelength.) The broader inhomogeneous distributions in these crystals is comparable to the 42 GHz inhomogeneous linewidth found previously in Bridgman-grown pentacene in *p*-terphenyl [28]. Finally, if the platelet is highly strained and cracked as sometimes occurs when it is epoxied to the end of an optical fiber, essentially no inhomogeneous line is observed. The excitation spectrum in this case shows only single molecules spread out over several hundred GHz in frequency space.

The widths of the individual pentacene peaks in Fig. 3 are laser power dependent, and attain the lifetime-limited width at low intensities and temperatures. Figure 4 shows the low-intensity excitation spectrum for a single pentacene molecule in *p*-terphenyl at 1.5 K. The spectrum is obtained with an excitation power of 89 pW, and a corresponding intensity (in free space) of 0.4 ± 0.1 mW/cm^2. The solid line is a Lorentzian fit to the data with a full width at half maximum (FWHM) of 7.8 ± 0.2 MHz. This is equal to the lifetime-limited

width for pentacene molecules in *p*-terphenyl O_1 sites at 1.5 K, as previously determined by photon echo measurements on large ensembles of pentacene molecules [29,30].

By slowly translating the laser focal spot across the face of the crystal and obtaining spectra at each position, we observe single molecule peaks localized in both frequency and position. Figure 5 shows a wire plot of spectra taken at a series of overlapping laser spots displaced 0.568 μm apart. Within the 300 MHz tuning range shown, the stable single molecule excitation peaks occurring at laser detunings of +20, +130 and -120 MHz appear at different positions in the crystal of 30, 35, and 40 μm. The shape of an excitation peak along the position axis is a direct measure of the (Gaussian) intensity profile of the laser beam in the crystal, as probed with the fluorescence emitted by a single molecule. In Fig. 5, the spatial width of a single-molecule peak, and hence that of the laser focal spot is $\simeq 5 \pm 0.5\,\mu$m FWHM. The fluorescence peaks have different sizes because the molecules do not pass directly through the center of the laser focus, and experience different peak laser intensities. The frequency widths of the peaks in Fig. 5 are slightly larger than the lifetime-limited width in Fig. 4 due to the use of an intensity somewhat above the saturation intensity for this measurement, but this saturation effect has been included in the spot size determination.

The intensity saturation behavior for several individual class I and class II pentacene defects in *p*-terphenyl O_1 sites at 1.5 K is shown in Fig. 6. The laser spot size was determined for each of the molecules in Fig. 6 by translating the beam as in Fig. 5. Each molecule in turn was positioned at the center of the laser focus by displacing the focal spot in two dimensions while monitoring a fluorescence peak. The free space peak intensity at the center of the laser focus could then be calculated from the standard Gaussian beam relation $I = 2P/\pi(D_{FWHM}/1.18)^2$, where P is the power in the laser beam at the sample, and D_{FWHM} is the FWHM diameter of the intensity profile. Figure 6 (a) shows single molecule linewidth

(FWHM) broadening and Fig. 6 (b) shows peak fluorescence emission saturation with excitation intensity. The total fluorescence emission rate (right ordinate in Fig. 6 (b)) is obtained from the detected fluorescence count rate (left ordinate) using the overall collection and detection efficiency factor D calculated in section II. The linewidths reached in the low intensity limit of Fig. 6 (a) reach 7.3 ± 0.8 MHz, in agreement with the lifetime-limited value (see also Fig. 4). In the high intensity limit, the peak fluorescence emission rate saturates at $(7.2 \pm 0.7) \times 10^5$ photons/second (Fig. 6 (b)). As the peak emission rate saturates, the emission rate in the wings of the excitation spectrum continues to increase with intensity, and the linewidth broadens as in Fig. 6 (a). The solid curves are fits to the data, which are described more fully in Section IV.

The linewidths (FWHM) of single (class I or class II) pentacene molecules also broaden with temperature as shown in Fig. 7. Below 4 K, the optical linewidth of pentacene molecules in *p*-terphenyl O_1 sites remains essentially constant at the lifetime-limited value of 7.8 MHz. Above 4 K, temperature-dependent dephasing processes contribute to the linewidth. As shown in Fig. 7, dephasing increases the linewidth by a factor of 100 over 4 K to 10 K. In previous photon echo experiments, the echo decay time temperature dependence for pentacene in various *p*-terphenyl sites was found to follow a form described by dephasing via a single pentacene librational mode[31]. The data in Fig. 7 are fit with this form of dephasing:

$$\Delta\nu_{FWHM} = \frac{1}{\pi T_2} = \frac{1}{2\pi T_1} + \frac{e^{-\Delta E/kT}}{\pi T_2'(\infty)} \qquad (1)$$

where the lifetime limited (T_1) width is $1/2\pi T_1 = 7.8 \pm 0.2$ MHz, the librational energy is $\Delta E/k = 38 \pm 1$ K $= 27 \pm 0.7$ cm^{-1} with k as Boltzmann's constant, and the pure dephasing prefactor is $1/\pi T_2'(\infty) = 33{,}500 \pm 4000$ MHz or $T_2'(\infty) = 9.5$ ps. The limiting optical linewidth, libration energy, and $T_2'(\infty)$ are in agreement with previous results[13, 31,32].

Numerous attempts were made to induce persistent spectral hole-burning, that is, light-induced changes in resonant frequency, for class I pentacene defects. Typically, a molecule was irradiated with the laser frequency fixed at the resonance frequency with powers as high as 1.6 μW for times up to 10 min, or scanned and detected at regular intervals over up to 55 min. No spectral hole-burning was observed; by using the peak excitation rate and the estimated total number of excitations, an upper bound can be placed on the hole-burning quantum efficiency of $\simeq 1 \times 10^{-9}$.

B. Spectroscopy of spectrally diffusing class II pentacene defects

A close examination of the peaks in the spectral landscape of Fig. 5 shows that in addition to the stable, single molecule peaks, there are also features that have a time dependence, i.e., that change from scan to scan. To examine the time-dependent features, a time sequence of excitation spectra are obtained without moving the fixed focal volume as in Figure 8. The spectra contain three time-independent class I peaks, which form stable ridges along the time axis near -130, -70, and +10 MHz. In the 0 to 150 MHz region is a single class II defect whose frequency varies from one scan to the next. Indeed, this same molecule can appear several times in the same 2 min laser scan, or almost not at all. Notice that in the same $\simeq 50$ μm^3 volume of crystal and at nearly the same frequency there are both class I defects as well as spectrally migrating class II defects. We broadly use the term "spectral diffusion" to refer to the changes in resonant frequency that occur as a function of time for class II single pentacene defects.

When the laser frequency as well as the position of the focal volume is held constant, then the time dependence of the peak fluorescence for a class I or a class II defect is measured, as in Fig. 9. In Fig. 9 (a), the laser is tuned near the peak of a stable class I defect, and the fluorescence signal remains essentially constant (the downward drift is most

likely due to a small amount of relative frequency drift between the laser and molecule). In Fig. 9 (b), the laser frequency is fixed in the vicinity of a time varying molecule. The collected fluorescence turns on and off discontinuously like a random telegraph [33] or quantum jump [34] signal as the molecule spectrally jumps into and out of resonance with the fixed laser frequency.

When the excitation power level is varied at a fixed frequency and focal spot position, the rate of spectral jumps does not appear to be influenced, as shown in Fig. 10. The measured fluorescence as a function of time is shown for a single pentacene defect at laser power levels of 0.89 nW in Fig. 10 (a) and 36 nW in Fig. 10 (b). The vertical scales in Fig. 10 (a) and (b) differ by a factor of 5.3 for the factor of 40 change in power level. (The corresponding intensities may be estimated from the ratio of fluorescence signal sizes and the ratio of power levels to be 0.3 and 11 mW/cm^2.) The number of jumps in Fig. 10 (a) and (b) are 10 and 13, which correspond to mean times between jumps of 80 and 61 seconds. The mean time between jumps does not decrease by the factor of 5.3 increase in fluorescence excitation. Hence, the spectral jump rate does not appear to be influenced by the optical excitation rate and thus cannot be regarded as a light-induced process that can produce spectral hole-burning. The change in resonant frequency for class II defects appears to be a spontaneous process.

The absence of fluorescence (dark periods) in Figs. 9 and 10 only means that the defect is not absorbing at the laser frequency. To follow the shifts in resonance frequency directly, we scanned more rapidly and sacrificed SNR in order to measure the spectral position of the defect once each second. Fig. 11 (upper part) shows how the resonance frequency of a spectrally jumping class II defect evolves with time, where each trace has been digitally smoothed. A digital waveform recorder locates the peak in each scan and records this resonance frequency as a function of time as a trend in the lower part of Fig. 11. For this

defect, the optical transition energy appears to have a preferred set of values and performs spectral jumps between these values that are discontinuous on the 1 second time scale of the measurement. This type of jumping behavior occurred for some tens of class II defects. In addition, one single molecule was observed which discontinuously jumped between two allowed frequencies, but a larger number of allowed frequencies was much more common (see below).

The behavior shown in Fig. 11 shows relatively discontinuous resonant frequency changes, but in fact a wide array of characteristics has been observed in our samples. Before illustrating other types of behavior, one crucial observation must be presented: class II defects have only been observed in the wings of the inhomogeneous line, i.e.. in those local environments that have high or low values of local strain such that their resonance frequency is far from the most common value. Further, the fraction of single molecules showing class II behavior increases for wavelengths further and further from line center. For example, using three different samples with inhomogeneous linewidths on the order of 10-20 GHz and observing 133 different single molecules, the fraction of class II increases from 13% at -38 GHz from line center, to 23% at -55 GHz, to 40% at -196 GHz from line center. Moreover, in a lightly doped unstrained sample with a 2 GHz wide inhomogeneous line, no class II defects were observed in the range from -2 GHz to -8 GHz from line center.

To illustrate spectral diffusion behavior different from that in Fig. 11, Fig. 12 shows the peak frequency trend of another pentacene defect over a 1.6 hour time period at 1.5 K. For this defect which is on the low frequency side of the inhomogeneous distribution, the overall trend is to creep in successive jumps towards higher optical frequencies. As shown in the inset in Fig. 12, there are residence times on the order of 30 seconds, with the molecule appearing at new, higher preferred frequencies at later times. This "creeping" pentacene

defect may be in an environment that is structurally relaxing at 1.5 K to an environment more typical of those found at the center of the inhomogeneous line.

One important physical measurement that would help to identify the source of the spectral diffusion effect would be temperature dependence of the jump rate. Since different molecules have different spectral jumping behavior, it is essential to try to follow the jumping dynamics of the same molecule over a reasonable temperature range, say 1.5-10 K, before the molecule jumps out of the range of the laser scan. Attempts to record careful temperature dependence with the lens focusing arrangement of Fig. 1 were generally unsuccessful, since during the transition from superfluid immersion at 2.18 K to a cold He gas environment, the focal length and therefore the focal volume itself would change dramatically preventing the continuous recording of excitation spectra for the same molecule. (No large change in jumping rate was observed between 1.5 K and 2.1 K.) This problem was partially alleviated by using the alternate sample configuration mentioned in Section II, where the sample is epoxied to the end of a cleaved single mode optical fiber ($\simeq$ 5 μm core diameter). In this configuration, an even broader array of spectral diffusion behaviors was observed, perhaps due to additional strain in the sample mounting.

Figures 13 and 14 show attempts at studying the jump rate dependence on temperature using a sample mounted on the end of a fiber. Figure 13 shows the peak frequency trend for a single class II defect at 1.5 and 4.0 K. This "wandering" defect spectrally diffuses rapidly, and is found at a new frequency in every one of the 2.68 second laser scans. Since it spectrally jumps as often or more often than once in each laser scan, its trend has a wandering appearance. During the 1600 second trend at 1.5 K (Fig. 13 (a)), the spectral wandering for this defect is confined to a 500 MHz region. At 4.0 K (Fig. 13 (b)), the wandering range is enlarged to 700 MHz. The spectral diffusion rate also appears to be

higher at 4.0 K. This could be due to a larger number of small jumps between the 2.68 second laser scans, or the spectral jump sizes may have increased with temperature.

Figure 14 shows the peak frequency trends of another class II defect at 4.18 and 5.77 K. Fig. 14 (a) shows the trend at 4.18 K in a time period of 5000 seconds. Pieces of the 4.18 K data in Fig. 14 (a) are expanded in Fig. 14 (b) and (c) for comparison with the shorter trend at 5.77 K in Fig. 14 (d). The residence time between the largest jumps is 80 seconds at 4.18 K, and 40 seconds at 5.77 K. This defect did not have a tendency to creep in any specific frequency direction, and was confined to a 300 MHz region at 4.18 K (compare this with Fig. 12). At 5.77 K this frequency region initially expanded to 400 MHz. After the 800 second time interval shown in Fig. 14 (d), this defect began to diffuse rapidly outside this 400 MHz region to lower frequencies and became confused with other nearby molecules. The difficulties of recording careful temperature dependence of class II molecules could be alleviated somewhat in future measurements by utilizing lower rather than higher temperatures.

IV. Analysis and Discussion

A. Evidence for single molecules of pentacene

The excitation spectra reported here are not likely to have resulted from molecules other than pentacene that may be impurities in low concentration in the starting material, because other aromatic hydrocarbons that might have survived the sublimation process (e.g., tetracene, perylene, etc.) have electronic absorptions extremely far away in frequency space from the pentacene 0-0 electronic origin. Further evidence in favor of the single-molecule interpretation is the fact that the observed spectra occur as isolated, near-delta-functions in the excitation spectrum, well above the background level. Inspection of Fig. 3 shows that

when several molecules have nearly degenerate resonance frequencies, the shape of the excitation spectrum is quite different. In addition, the low-power, low-temperature linewidth for both class I and class II single molecules (Fig. 4) reach the 7.8 MHz lifetime-limited width that would be expected from earlier photon echo[31] measurements of T_2 and the temperature dependence of the dephasing agrees with earlier measurements for large ensembles of pentacene in *p*-terphenyl[29] (Fig. 7). Further, translation of the laser spot shows narrow fluorescence excitation features localized in space (Fig. 5).

One may consider the possibility that spectra like Fig. 4 result from the highly unlikely situation of two or more molecules with resonance frequencies that are identical to within $\simeq$ 1 MHz. The strength of the fluorescence emission is approximately that which would be expected for a single molecule; however, attempting to quantify this absolute determination of fluorescence strength to better than a factor of two or so is quite difficult. Perhaps the strongest proof that the observed spectra represent single impurity species are the observations of discontinuous spectral jumping shown in Figs. 8-14. If there were several different molecules at the same frequency experiencing stochastic perturbations in resonance frequency, such clear spectral jumps would wash out into an ill-defined broadening of the spectral profile, which is definitely not what is observed.

A further possibility to consider is whether or not the spectra result from dimer pairs, even though dimers are extremely unlikely at the low concentrations used. In this case, one would expect that the coupling between the molecules of the dimer would alter the low-temperature linewidth or the dephasing characteristics, as has been shown for several of the more common dimers[30]. We cannot totally rule out, however, that some of the spectra observed are indeed dimers with extremely weak coupling.

A final possibility is that the single-molecule spectra in the wings of the inhomogeneous line result from molecules near the surfaces of the samples, since the local strain values on

the surface would be expected to be quite different from the strain values in the bulk. This explanation is incomplete, however, since single-molecule spectra occur on both the red and blue edges of O_1 and O_2, as well as quite near line center in samples with very low concentration. (Class II behavior is also observed both to the red and blue of the inhomogeneous line, but not at line center.) At the present time, the evidence in favor of the single-molecule character of the observed spectra is substantial. However, by searching for spectra with different characteristics, it is certainly possible that future measurements can probe either dimers or molecules on the surface of the sample.

B. Saturation Behavior

The observations of single molecule spectra reported here have required integration times long compared to any internal time constants, such as the triplet lifetime τ_T or the first excited singlet dephasing time T_2. Since by the ergodic theorem there should be an equivalence between ensemble averaging for an assembly of identical molecules and long time averaging for a single defect, one possible method for analyzing the single molecule saturation data is to use density matrix theory. Three-level density matrix theory for a molecule which includes intersystem crossing to a long lived triplet state has been formulated[35]. Since inhomogeneous broadening is not present for the absorption spectrum of a single molecule, it is not necessary to perform integrations over an assumed spectral density for an inhomogeneous distribution. After simple algebraic manipulations of Eqs. (16) - (18) of Ref. 35 in steady state, the excitation linewidth (FWHM) $\Delta\nu_{FWHM}$ and the fluorescence emission rate R for a single molecule can be written

$$\Delta\nu_{FWHM}(I) = \Delta\nu_{FWHM}(0)\left[1 + I/I_S\right]^{\frac{1}{2}} \tag{2}$$

$$R(I) = \rho_{22}\frac{1}{\tau_F}\phi_F = R_\infty \frac{I/I_S}{1 + I/I_S} \tag{3}$$

where $\tau_F = (k_{21} + k_{23})^{-1}$ is the fluorescence lifetime with standard notation for the rate constants and with the subscripts 1, 2, and 3 referring to the ground state, the first excited singlet, and the triplet state, respectively, and ϕ_F is the fluorescence yield. The three level saturation intensity appearing in the density matrix treatment (MKS units, ignoring local field corrections at the defect) is

$$I_S = \frac{\varepsilon_o c\hbar^2(k_{21} + k_{23})}{|\mu_{21}|^2(2 + A)T_2} \tag{4}$$

where μ_{21} is the projection of the dipole moment along the electric field, $A = k_{23}/k_{31}$, and the fully saturated fluorescence emission rate is

$$R_\infty = \frac{(k_{21} + k_{23})\phi_F}{2 + A}. \tag{5}$$

The solid curves in Fig. 6 are fits to the data using Eqs. (2) and (3). Two of the parameters, the low power limiting linewidth $\Delta\nu_{FWHM} = 7.3 \pm 0.8$ MHz and the fully saturated fluorescence photocount rate $D \times R_\infty = 8100 \pm 300$ counts/second (yielding $R_\infty = (7.2 \pm 0.2) \times 10^5$ photons/second), can essentially be read from Fig. 6. The remaining parameter, $I_S = 2.5 \pm 0.8$ mW/cm^2, fits the intensity dependence of both the linewidth and emission rate data.

The values of R_∞ and I_S derived from these measurements on single pentacene defects may be compared to values for these quantities computed from photophysical experiments on ensembles of many molecules. The fully saturated emission rate R_∞ may be calculated from Eq. 5 to be 3.1×10^7 s^{-1} using $k_{21} + k_{23} = 4.6 \times 10^7$ s^{-1} [30], $k_{31} = 2.2 \times 10^4$ s^{-1} [24], a fluorescence yield of $\phi_F = 0.08$ [36], and a triplet yield ϕ_T of 0.0047 [24]. The calculated value is within a factor of two of the value of R_∞ determined from Fig. 6, which is quite reasonable agreement considering that absolute fluorescence determinations can be hard to quantify.

On the other hand, the value of I_s expected from Eq. 4 using the previously determined dipole moment of 0.7 Debye is 51 mW/cm², quite different from the measured value of 2.5 mW/cm². The reason for this discrepancy is unknown. One possible source could be systematic error in our intensity calibrations. While absolute intensity values are often hard to measure, in this case the shape of the Gaussian beam profile and the peak intensity have been determined fairly well using a single molecule as a probe of the light beam, and the laser power meters have been compared to a standard thermopile. Another possible source is the neglect of local field factors in Eq. 4, but such factors usually only change the overall value by 50%. A third possibility is that the photophysical parameters are modified; this is unlikely because good agreement is found using the same photophysical parameters to calculate R_∞ from Eq. (5). Finally, it may be that a more detailed theory such as the Redfield approach[37] or a theory with proper inclusion of the AC Stark effect for a three-level system is essential for the proper description. It is clear that a good deal of nonradiative decay relaxes the excited state of pentacene in *p*-terphenyl, since $\phi_F + \phi_T < 1$. It may be that this nonradiative decay channel is altered for a single molecule. It is hoped that presentation of these results will stimulate further theoretical interest in this problem.

C. Spectral Hole-Burning

The results in Section III for both class I and class II single pentacene defects do not support the observation of spectral hole-burning. One is thus led to consider what might have been the source of the spectral hole-burning observed during the earlier study of SFS for pentacene in *p*-terphenyl[11]. The SFS studies utilized the powerful absorption technique of FM spectroscopy to observe the small spectral variations on a zero background. In fact, the size of the observed spectral holes even after extended irradiation were on the order of 1 part in 1000 of the total absorption. One interpretation of this result is that of all the pentacene molecules with center frequencies within one homogeneous linewidth of the laser

frequency, only 0.1% had a photoinduced pathway leading to changes in resonance frequency. Other interpretations are possible given that detailed study of the spectral hole-burning phenomenon has not been reported.

If it is correct that only 0.1% of all molecules can participate in hole-burning, then in the single-molecule regime one might expect on average to find a molecule capable of light-induced resonant frequency changes for only one in a thousand molecules, and to date, only several hundred single molecules have been studied in detail. It is therefore quite possible that specific single molecules will be found that clearly undergo photoinduced spectral changes. It will be most interesting to perform detailed study of the local environment around such molecules using Stark, stress, Zeeman, and other perturbations to determine the symmetry and interactions that lead to spectral hole formation.

D. Spectral Diffusion

In contrast to the scarcity of single molecules able to under go hole-burning, the appearance of single molecules of pentacene in *p*-terphenyl which spontaneously change resonant frequency with time (class II centers) is much more common. This surprising observation of spectral jumping may be analogous to spectral diffusion processes that play a crucial role in the physics of glasses and other amorphous materials[38]. Here, the single-molecule technique allows the detailed spectral changes to be followed in real time for only one center, without any averaging over an inhomogeneous distribution that may obscure the effect. The spectral changes take many forms, from discontinuous jumping, to quasi-continuous wandering, to creeping toward line center in small discontinuous jumps. The fraction of spectrally diffusing molecules clearly increases with distance from the center of the inhomogeneous line. Thus, the occurrence of class II defects appears to be associated

with sites that have some degree of local disorder so that the local strain or electric field is far from the equilibrium value.

Since the resonance frequency of a single molecule in a solid is extremely sensitive to the local strain (and other local fields) at the position of the molecule, the spectral jumps may occur because the class II pentacene molecules are coupled to an (unidentified at present) set of degrees of freedom in the nearby host crystal that are excited at 1.5 K. Further, these degrees of freedom interact with phonons, as evidenced by the increase in jumping rate and range at higher temperatures (Figs. 13 and 14). Unfortunately, the diversity of behavior observed has made a detailed determination of the temperature dependence of questionable valuc at this time.

One possible source for the effect could be librational tunnelling of the central phenyl ring of the nearby *p*-terphenyl molecules about the *p*-terphenyl molecular axis. To explain this suggestion, it is helpful to review the properties of the equilibrium *p*-terphenyl crystal. At room temperature, the central ring has a large librational amplitude indicating oscillation in a double-well potential[39]; however, below 113 K the librational motion effectively ceases since the barrier height is over 200 cm^{-1} [40]. The specific equilibrium orientations of the central ring for each of the four molecules in the unit cell have been described[39]. This suggests that the central ring becomes locked in a specific orientation determined by the minima of an asymmetric double-well potential.

The spectral diffusion effects reported here may therefore result from discrete librational motions of the central phenyl ring of *p*-terphenyl driven by phonon assisted tunnelling[41] in an asymmetric double-well potential that has become allowed due to the local disorder. In this picture, the spectrally diffusing pentacene molecule is surrounded by a set of two-level systems (TLS), where the instantaneous pentacene resonance frequency is determined by the complete set of quantum numbers describing the state of each of these two-level systems.

This sort of model is appealing, in that it is easy to see why both discrete jumping among only a few allowed frequencies (Fig. 11) and jumping among many states with small spacings (Fig. 13) can both occur, depending on the number of TLS's near the pentacene and the distance between each TLS and the molecule. More detailed temperature studies on one single molecule with well-defined diffusion dynamics might allow the determination of the type and number of TLS's that are interacting with this center. However, a different set of local TLS's may be required for another spectrally diffusing molecule.

Other possible sources for the class II spectral diffusion behavior may be postulated. Helium atom or perhaps even *p*-terphenyl vacancy diffusion may occur in those regions of the crystal responsible for the wings of the inhomogeneous line. It is also possible that during nonradiative decay, anharmonic local modes [42] normally bound to class II defects are released to propagate in the lattice. It is clear that further experiments are necessary to conclusively identify the molecular motions responsible for the spectral diffusion effect for pentacene in *p*-terphenyl.

V. Conclusion

This paper has reported detailed spectroscopic measurements on single molecules of pentacene in *p*-terphenyl using fluorescence excitation spectroscopy. The high signal-to-noise ratio has allowed measurement of the properties of molecules that have time-independent resonance frequencies, and molecules whose resonant frequency changes spontaneously with time (spectral diffusion). The measurements have included determination of the lifetime-limited width and temperature dependence of the dephasing, both of which are in agreement with previous results. The saturation behavior of the optical linewidth and fluorescence emission rate follow a standard homogeneous three-level model, although the

value of the saturation intensity is lower than expected from independently measured photophysical parameters.

Class II spectrally diffusing molecules undergo spontaneous changes in resonance frequency at 1.5 K and higher. In fact, each spectrally diffusing molecule has a unique character, with behavior ranging from discontinuous jumping, to wandering, to creeping in frequency space. It has been hypothesized that these spectral variations are due to phonon-assisted transitions of two-level systems or other degrees of freedom in the nearby *p*-terphenyl host of unknown character. In any case, the new techniques of optical spectroscopy of single molecules in solids has led to the observation of a menagerie of physical effects for single pentacene molecules in *p*-terphenyl.

The attainment of single-molecule detection and spectroscopy in solids opens up a new frontier of single-absorber experiments in which the measured properties of the absorbing center are not averaged over many "equivalent" absorbers. Here the absorbing entity is exquisitely sensitive to the symmetry and perturbations introduced by the local environment such as the local vibrational modes and the true local fields. While as a general technique the method presented here may not be applicable to all molecular impurities, it can be applied to the large number of absorbing ions and molecules in solids that have zero-phonon transitions and strong absorptions, ideally with large fluorescence emission efficiency. The detectability of the resulting single-center signal for specific systems must be evaluated in each case. It is clear, however, that further information about specific local environments will be forthcoming in future experiments on single impurities in solids.

Acknowledgements

The authors thank Prof. M. Fayer of Stanford University for details of the construction of the cosublimation apparatus. This work was supported in part by the U. S. Office of Naval Research.

References

• Present address: Los Alamos National Laboratory, Los Alamos, NM 87545

1. G. Binnig and H. Rohrer, *Rev. Mod. Phys.* **59**, 615 (1987).
2. H. Ohtani, R. J. Wilson, S. Chiang, C. M. Mate, *Phys. Rev. Lett.* **60**, 2398 (1988).
3. J. S. Foster and J. E. Frommer, *Nature* **333**, 542 (1988).
4. See for example W. M. Itano, J. C. Bergquist, and D. J. Wineland, *Science* **237**, 612 (1987) and references therein.
5. F. Diedrich, E. Peik, J. M. Chen, W. Quint, and H. Walther, *Phys. Rev. Lett.* **59**, 2931 (1987).
6. D. C. Nguyen, R. A. Keller, J. H. Jett, and J. C. Martin, *Anal. Chem.* **59**, 2158 (1987).
7. K. Peck, L. Stryer, A. N. Glazer, and R. A. Mathies, *Proc. Nat. Acad. Sci. USA* **86**, 4087 (1989).
8. E. B. Shera, N. K. Seitzinger, L. M. Davis, R. A. Keller, and S. A. Soper, *Chem. Phys. Lett.* **174**, 553 (1990).
9. S. A. Soper, E. B. Shera, J. C. Martin, J. H. Jett, J. H. Hahn, H. L. Nutter, and R. A. Keller, *Anal. Chem.* **63**, 432 (1991).
10. A. M. Stoneham, *Rev. Mod. Phys.* **41**, 82 (1969).
11. W. E. Moerner and T. P. Carter, *Phys. Rev. Lett.* **59**, 2705 (1987).
12. T. P. Carter, M. Manavi, and W. E. Moerner, *J. Chem. Phys.* **89**, 1768 (1988).
13. D. A. Wiersma, in *Photoselective Chemistry, Part 2*, J. Jortner, R. D. Levine, and S. A. Rice, eds. (*Adv. in Chem. Phys.* **47**) (Wiley, New York, 1981), pp. 421-485.
14. T. E. Orlowski and A. H. Zewail, *J. Chem. Phys.* **70**, 1390 (1979).
15. G. C. Bjorklund, *Opt. Lett.* **5**, 15 (1980).
16. R. Lange, W. Grill, and W. Martienssen, *Europhys. Lett.* **6**, 499 (1988).

17. W. M. Yen, in *Laser Spectroscopy of Solids II*, edited by W. M. Yen, Springer Topics in Applied Physics Vol. 65 (Springer, Berlin, Heidelberg, 1989), p. 23.

18. W. E. Moerner and L. Kador, *Phys. Rev. Lett.* **62**, 2535 (1989).

19. W. E. Moerner and L. Kador, *Analy. Chem.* **61**, 1217A (1989).

20. L. Kador, D. E. Horne, and W. E. Moerner, *J. Phys. Chem.* **94**, 1237 (1990).

21. M. Orrit and J. Bernard, *Phys. Rev. Lett.* **65**, 2716 (1990).

22. W. P. Ambrose and W. E. Moerner, *Nature* **349**, 225 (1991).

23. W. E. Moerner and W. P. Ambrose, *Phys. Rev. Lett.* **66**, 1376 (1991).

24. H. de Vries and D. A. Wiersma, *J. Chem. Phys.* **70**, 5807 (1979).

25. J. H. Meyling and D. A. Wiersma, *Chem. Phys. Lett.* **20**, 383 (1973).

26. R. Pariser, *J. Chem. Phys.* **24**, 250 (1956).

27. G. C. Bjorklund and M. D. Levenson, *Phys. Rev. A* **24**, 166 (1979).

28. R. W. Olson and M. D. Fayer, *J. Phys. Chem.* **84**, 2001 (1980).

29. H. de Vries and D. A. Wiersma, *J. Chem. Phys.* **69**, 897 (1978).

30. F. G. Patterson, H. W. H. Lee, W. L. Wilson, and M. D. Fayer, *Chem. Phys.* **84**, 51 (1984).

31. W. H. Hesselink and D. A. Wiersma, *J. Chem. Phys.* **73**, 648 (1980).

32. F. G. Patterson, W. L. Wilson, H. W. H. Lee, and M. D. Fayer, *Chem. Phys. Lett.* **110**, 7 (1984).

33. C. W. Gardiner, *Handbook of Stochastic Methods* (Springer, Berlin, 1983) pp. 78-79.

34. W. Nagourney, J. Sandberg, and H. Dehmelt, *Phys. Rev. Lett.* **56**, 2797 (1986).

35. H. de Vries and D. A. Wiersma, *J. Chem. Phys.* **72**, 1851 (1980).

36. B. Soep, A. Kellmann, M. Martin, and L. Lindqvist, *Chem. Phys. Lett.* **13**, 241 (1972).

37. P. de Bree and D. A. Wiersma, *J. Chem. Phys.* **70**, 790 (1979).

38. B. Golding and J. E. Graebner, in *Amorphous Solids Low Temperature Properties*, W. A. Phillips, ed. (Springer, Berlin Heidelberg, 1981), pp. 118-120.

39. J. L. Baudour, Y. Delugeard, and H. Cailleau, *Acta Cryst.* **B32**, 150 (1976).

40. B. Wyncke, F. Brehat, and A. Hadni, *J. de Phys.* **38**, 1171 (1977).

41. J. A. Sussman, *Ann. Phys.* **6**, 135 (1971).

42. A. J. Sievers and S. Takeno, *Phys. Rev. Lett.* **61**, 970 (1988).

Figure Captions

Figure 1. *Sample optical assembly for single molecule fluorescence excitation in a solid at liquid helium temperatures.* The excitation laser beam enters from the left and is focused by a 10 mm focal length lens (L) into the sample (S), which is mounted on a NaCl plate. The excitation beam is terminated with a piece of black tape (B). 42 % of the fluorescence from the sample is collected by a paraboloid (P), which collimates the emission into a beam propagating to the right in the figure. Fine positioning of the lens (L) relative to the sample is accomplished with an electromagnetic actuator consisting of a coil (C) and magnet (M). Vertical displacement of the sample relative to the laser focal spot with 10 micrometer resolution is performed with a translation stage and micrometer screw (not shown).

Figure 2. Optical apparatus for laser focal spot translation and frequency calibration. The figure is described in the text.

Figure 3. Fluorescence excitation spectrum of pentacene in *p*-terphenyl at 1.5 K. Zero laser detuning is near the center of the O_1 site inhomogeneous distribution at 592.321 nm wavelength. (a) shows a single 10 min excitation spectrum obtained with 2 nW of laser power. (b) shows two spectra on an expanded scale (with the upper trace displaced from the lower) in the wing of the O_1 site inhomogeneous distribution. The single peaks out in the wing are excitation peaks for single pentacene defects.

Figure 4. Low power fluorescence excitation spectrum for a single pentacene molecule in a sublimed crystal of p-terphenyl at 1.5 K. 0 MHz detuning $\equiv$ 592.407 nm, which is in the wing of the O_1 site inhomogeneous line. The solid line is a Lorentzian fit to the data.

Figure 5. Single pentacene-defect fluorescence excitation spectral landscape in a crystal of *p*-terphenyl. This figure is a wire plot showing a sequence of spectra taken at different laser focal spots each displaced by 0.57 μm. Zero MHz detuning is at a laser wavelength of 592.544 nm, T = 1.5 K, laser power= 1.5 nW, and each spectrum was obtained over a 2 min period.

Figure 6. Single pentacene molecule saturation behavior. The fluorescence excitation linewidth (FWHM) (a) and fluorescence emission rate (b) are shown as a function of laser intensity at 1.5 K. The excitation wavelengths of these molecules are 592.332 nm (triangles, class I), 592.333 nm (circles, class I), and 592.572 nm (rectangles, class II). The solid lines are fits to the data as described in the text. The intensity is the free space intensity at the molecules' location without local field corrections.

Figure 7. Single pentacene molecule linewidth broadening with temperature. Rectangles are linewidth data taken with a laser focusing lens (L in figure 1) for molecules with excitation wavelengths of 592.334 nm, 592.342 nm, and 592.592 nm. Circles are data taken with a sample attached to an optical fiber with using an excitation wavelength of 592.370 nm. The solid line is a fit to the data described in the text. The molecule near 592.592 nm is a class II defect and the remainder are class I.

Figure 8. Single pentacene defect fluorescence excitation spectra time dependence. Upper half: wire plot of individual spectra, lower half: contour plot of same data obtained with 2 min per spectrum, laser power= 1.5 nW, and 0 MHz detuning $\equiv$ 592.539 nm. The appearance of class I at negative detunings and class II at positive detunings has no significance.

Figure 9. Pentacene fluorescence signals at fixed wavelengths for one stable and one spectrally jumping molecule. In the first 10 seconds of (a), the laser is tuned onto a molecule at 592.404 nm, and the detected fluorescence signal decreases slowly over 200 sec (probably due to laser drift). In (b), the laser wavelength is held at 592.405 nm, and the fluorescence signal jumps up and down as the single pentacene molecule jumps into and out of resonance.

Figure 10. Spectral jump rate power independence. Spectral jumps are observed in the fluorescence signal of a single pentacene defect with a fixed laser wavelength of 592.362 nm at laser powers of (a) 0.89 nW and (b) 36 nW. The single molecule emission rate increases by a factor of 5.3 (the (b) ordinate is increased by a factor of 5.3 for comparison) for the factor of 40 increase in excitation power.

Figure 11. Spectral jumps in the resonance frequency of a class II single pentacene defect. In the upper half of the figure are individual 1 second excitation spectra. The peak in each spectrum is recorded as a peak frequency trend in the lower half of the figure. Zero MHz detuning is at a wavelength of 592.546 nm.

Figure 12. Long term frequency creep for a spectrally jumping pentacene defect. The peak frequency of a class II defect near 592.544 nm (on the long wavelength side of the O_1 inhomogeneous distribution) spectrally jumps no more than 100 MHz on short time scales, but tends towards higher frequencies in successive jumps on a 1.6 hour time scale. The inset is an expanded 600 second portion of the trend showing the individual jumps of < 80 MHz in size.

Figure 13. Qualitative increase in spectral diffusion rate with temperature. Traces (a) and (b) are peak-frequency trends for a spectrally jumping molecule near 592.582 nm excitation

wavelength. This molecule jumps often, appearing at a new frequency in each 2.68 second laser scan. Raising the temperature from (a) 1.5 K to (b) 4.0 K appears to increase the spectral diffusion rate and range.

Figure 14. Qualitative increase in spectral jump rate with temperature. Peak-frequency trends for a single class II pentacene defect near 592.410 nm wavelength at a temperature of 4.18 ± 0.04K ((a), (b), and (c)), and at a higher temperature of 5.77 ± 0.02K (d). (b) and (c) are the 0 to 800 and 800 to 1600 second sections of the data in (a) expanded for comparison with the 0 to 800 second data at 5.77 K in (d). Note that the jump rate for the largest jumps at 5.77 K in (d) is nearly twice the jump rate at 4.18 K in (b) and (c).

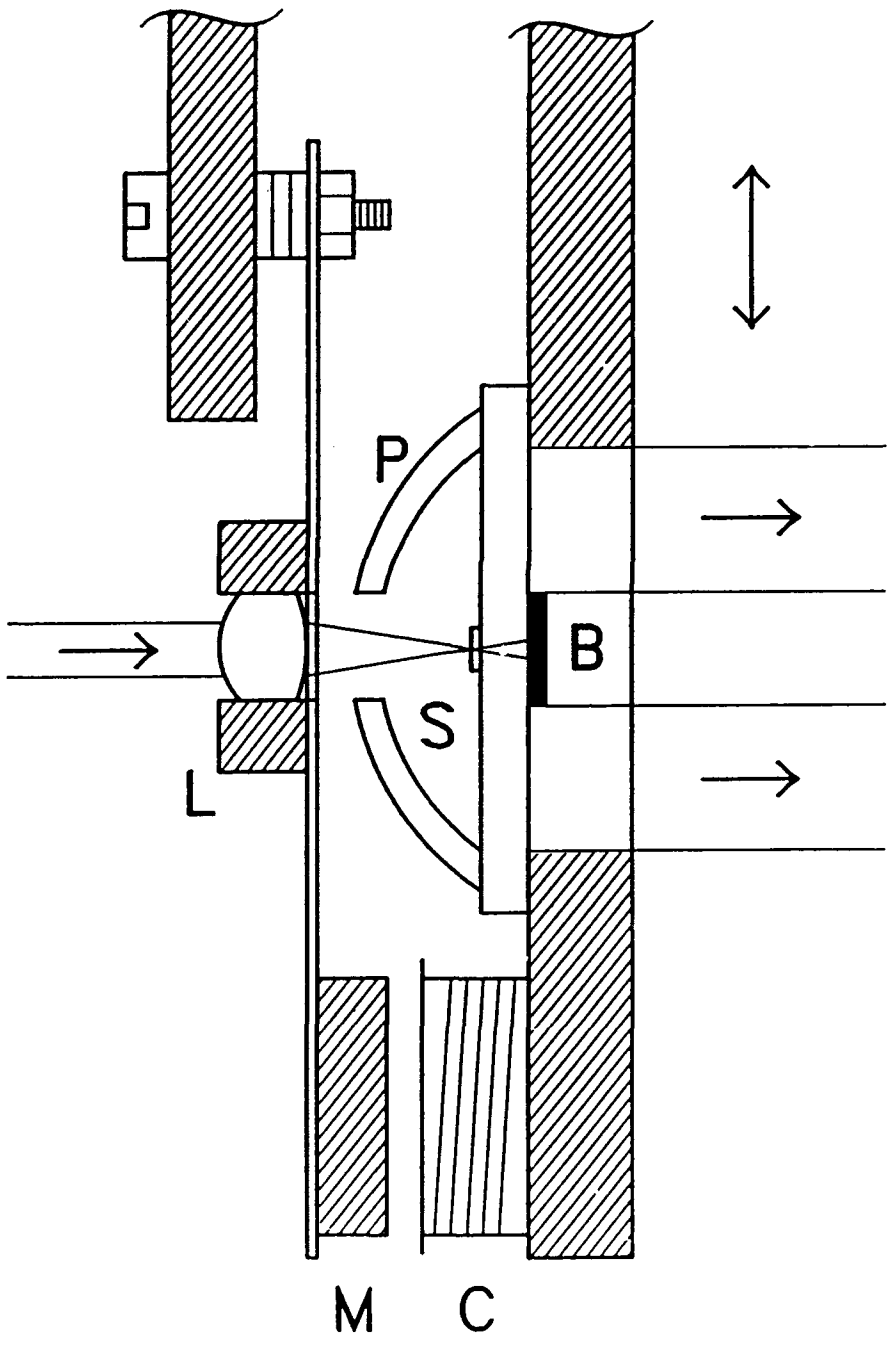

FIG. 1

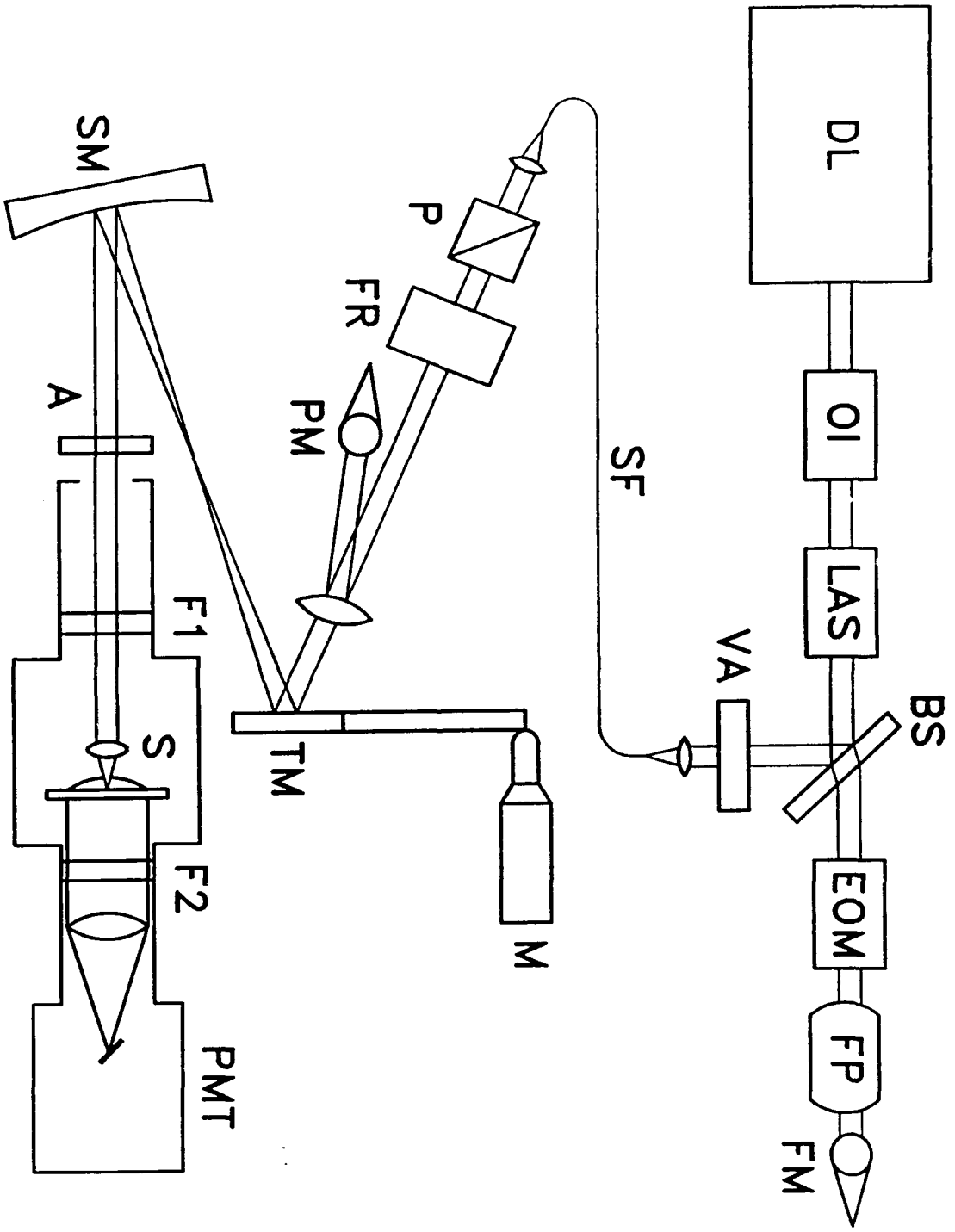

FIG. 2

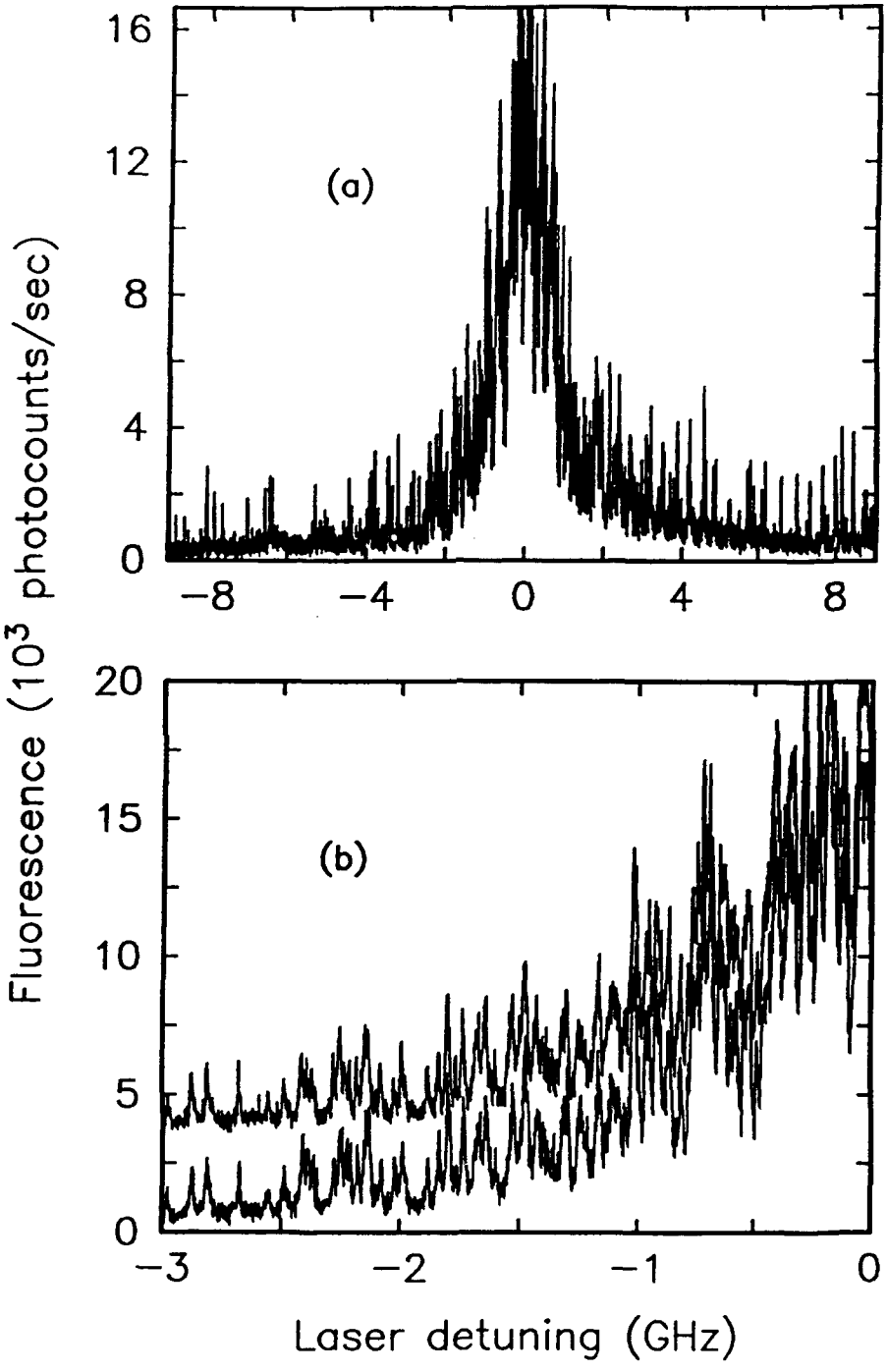
16
12
8
4
0
(a)
−8
−4
0
4
8
20
15
10
5
0
(b)
−3
−2
−1
0
Fluorescence (10^3 photocounts/sec)
Laser detuning (GHz)

FIG. 3

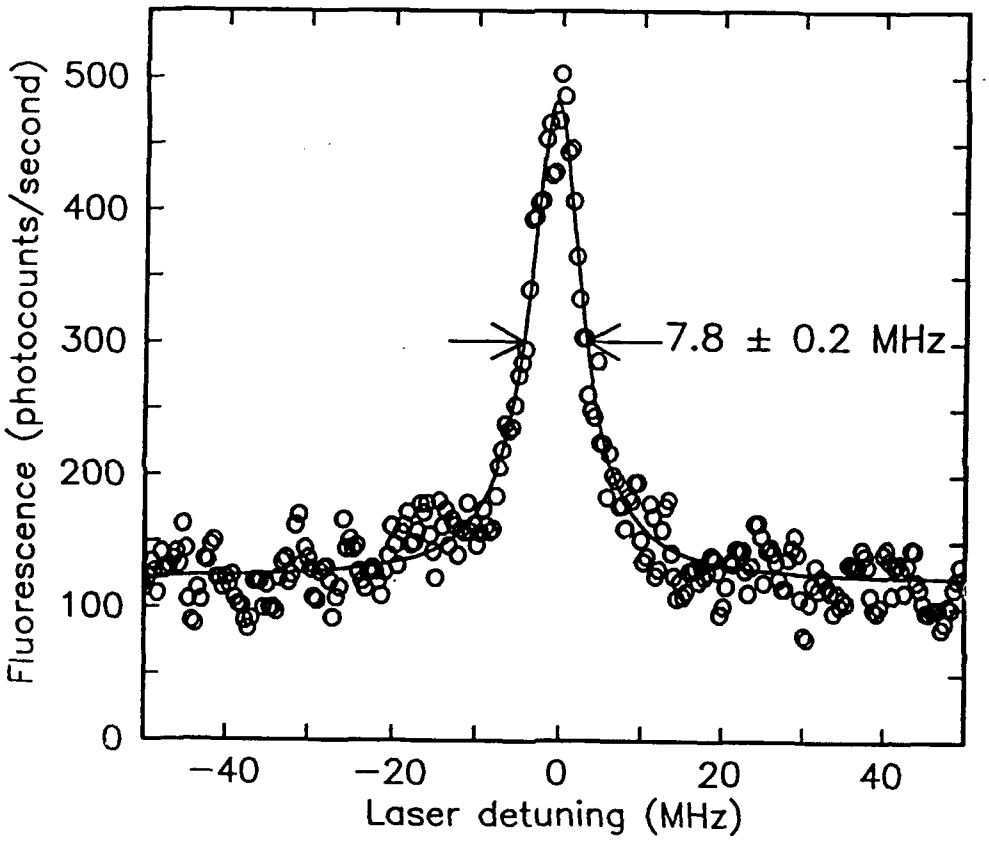
Fluorescence (photocounts/second)
500
400
300
200
100
0
−40
−20
0
20
40
Laser detuning (MHz)
7.8 ± 0.2 MHz

FIG. 4

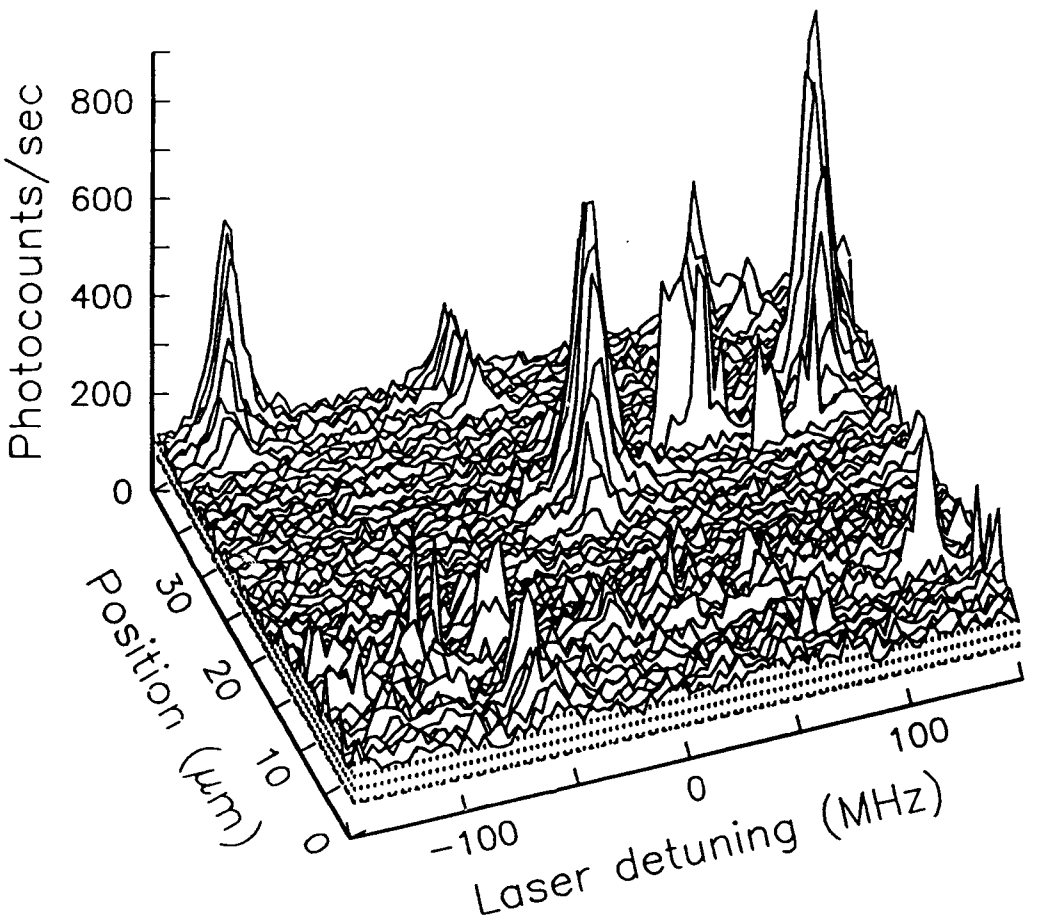
Photocounts/sec
800
600
400
200
0
Position (μm)
30
20
10
0
−100
0
100
Laser detuning (MHz)

FIG. 5

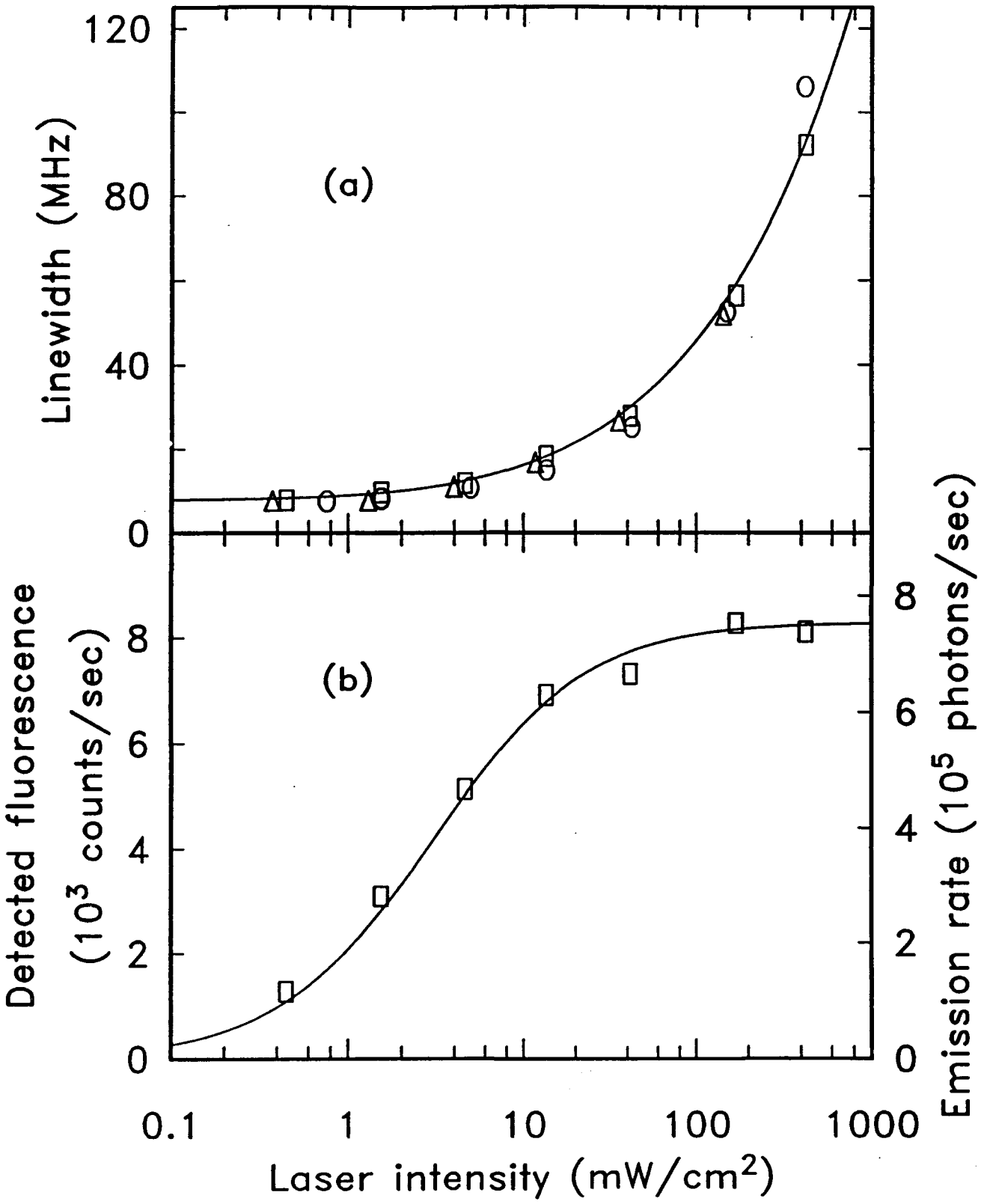
120
80
40
0
Linewidth (MHz)
(a)
(b)
Detected fluorescence
(10^3 counts/sec)
8
6
4
2
0
Emission rate (10^5 photons/sec)
0.1
1
10
100
1000
Laser intensity (mW/cm^2)

FIG. 6

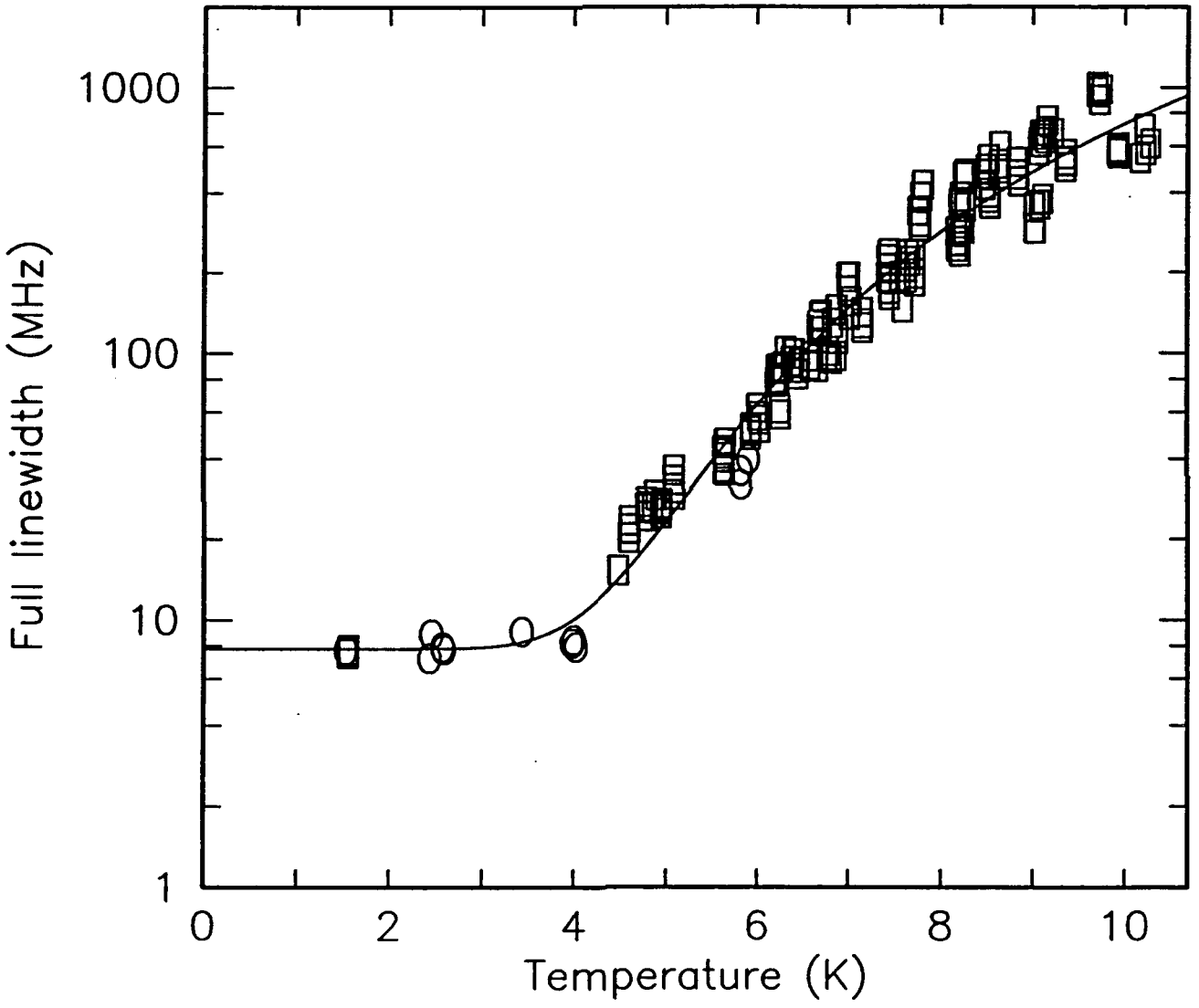

FIG. 7

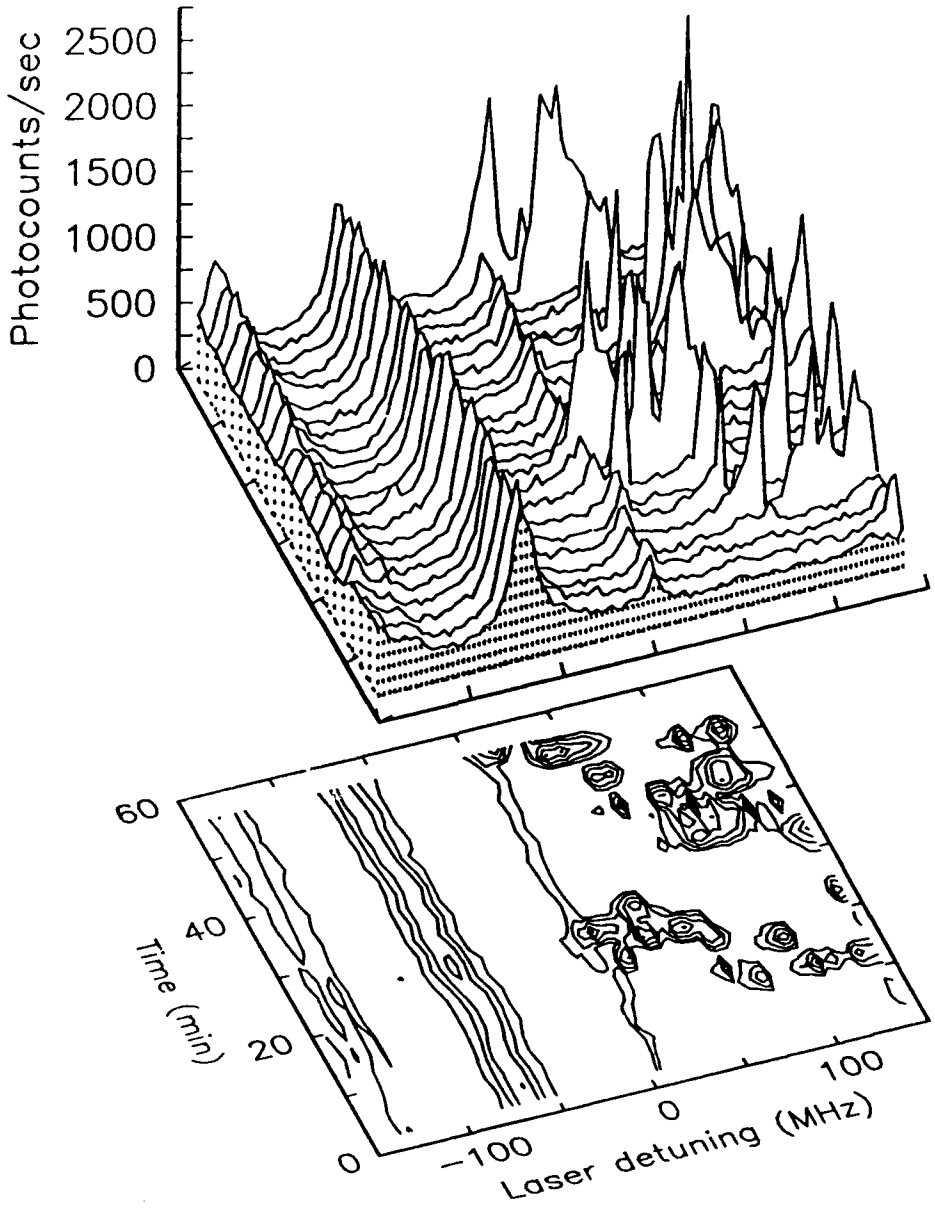
Photocounts/sec
2500
2000
1500
1000
500
0
60
40
20
0
Time (min)
-100
0
100
Laser detuning (MHz)

FIG. 8

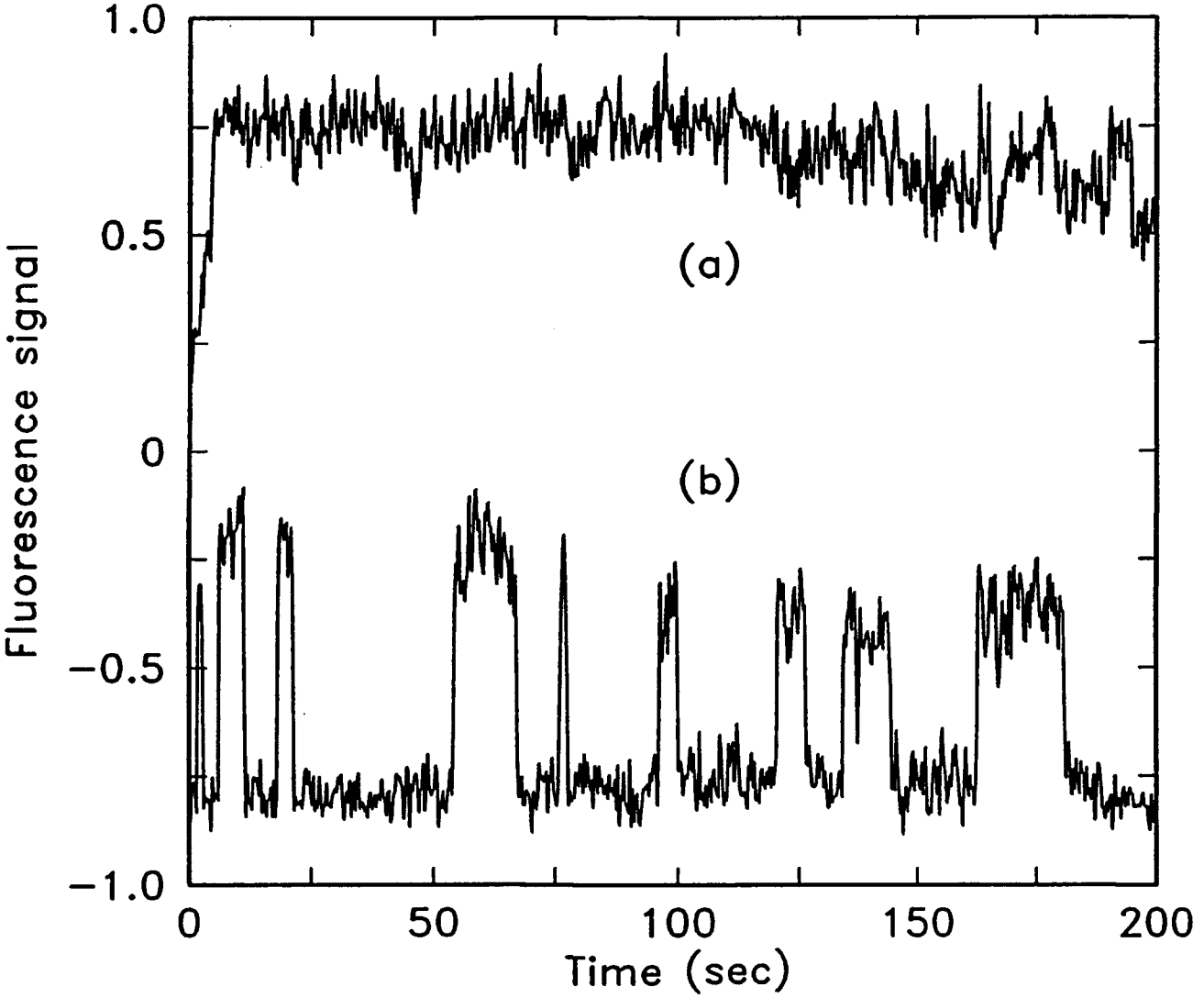

FIG. 9

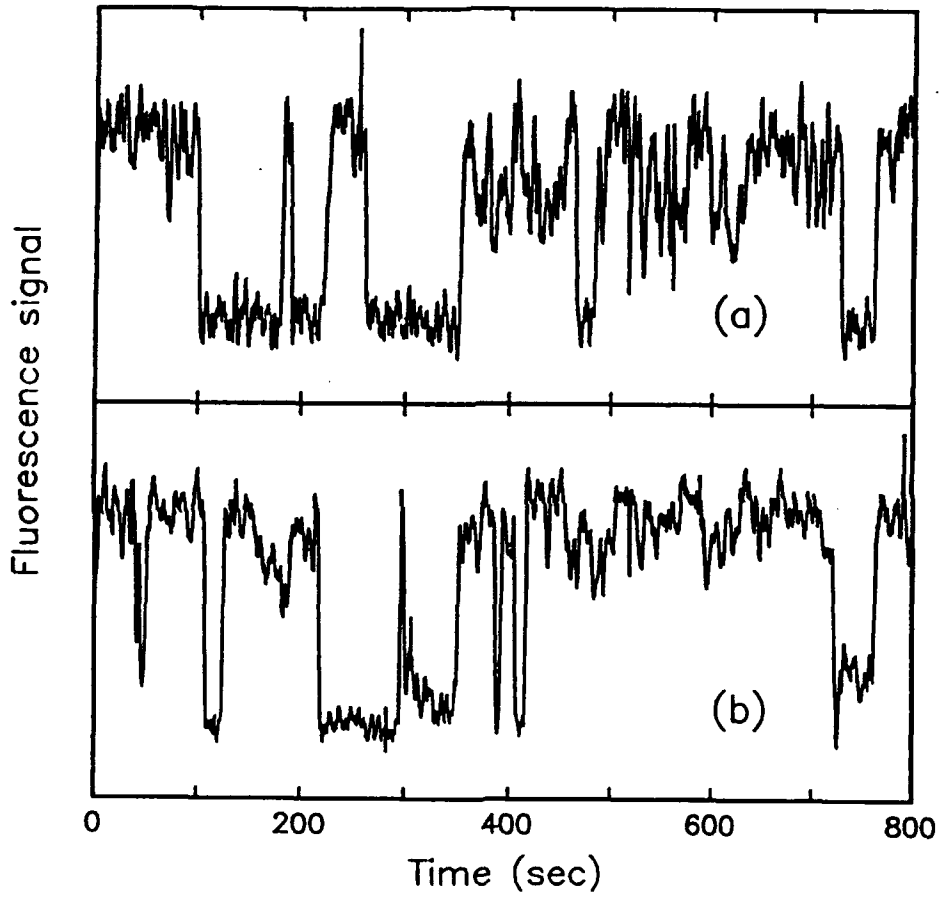

FIG. 10

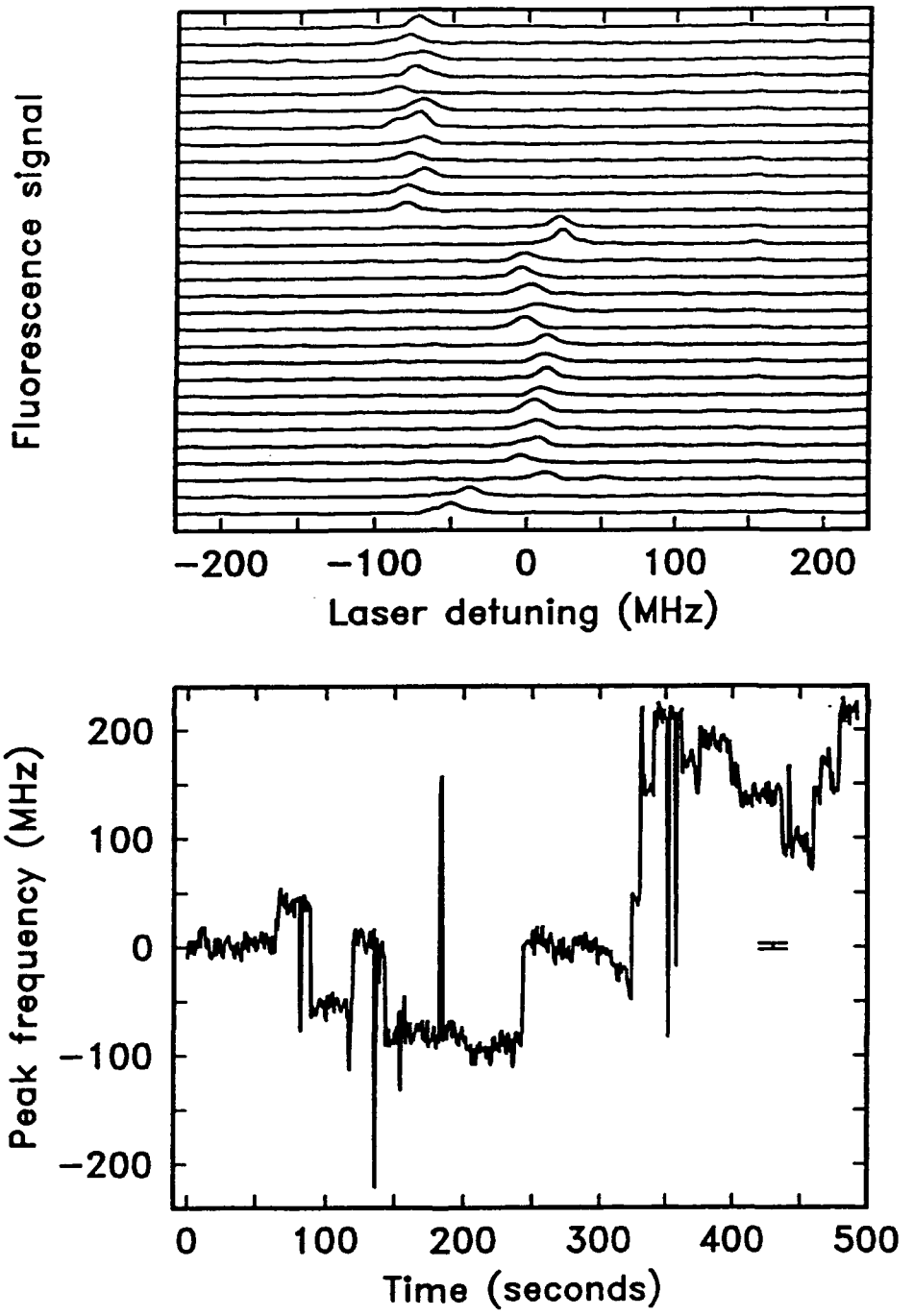
Fluorescence signal
−200
−100
0
100
200
Laser detuning (MHz)
Peak frequency (MHz)
200
100
0
−100
−200
0
100
200
300
400
500
Time (seconds)

FIG. 11

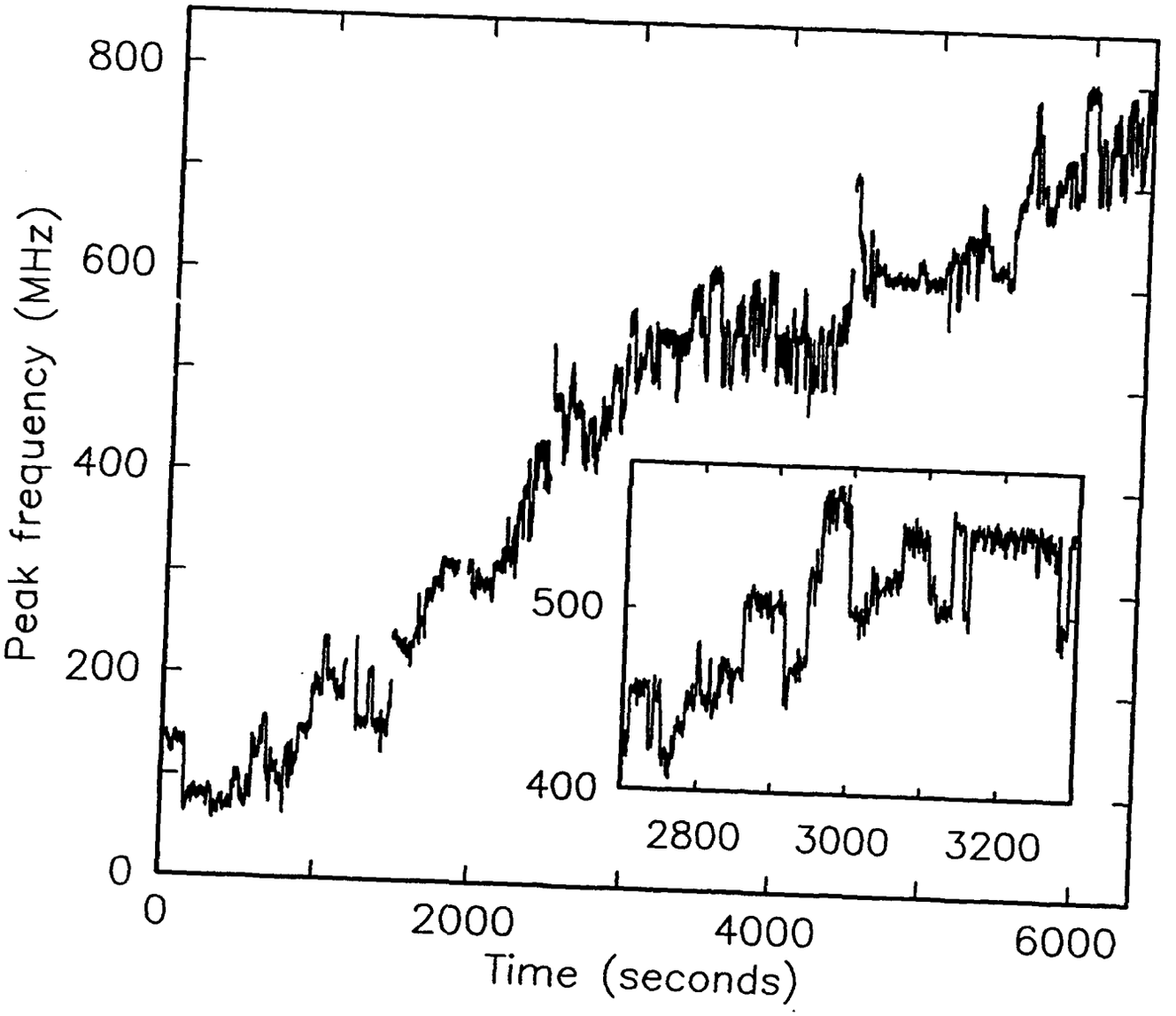
800
600
400
200
0
Peak frequency (MHz)
0
2000
4000
6000
Time (seconds)
500
400
2800
3000
3200

FIG. 12

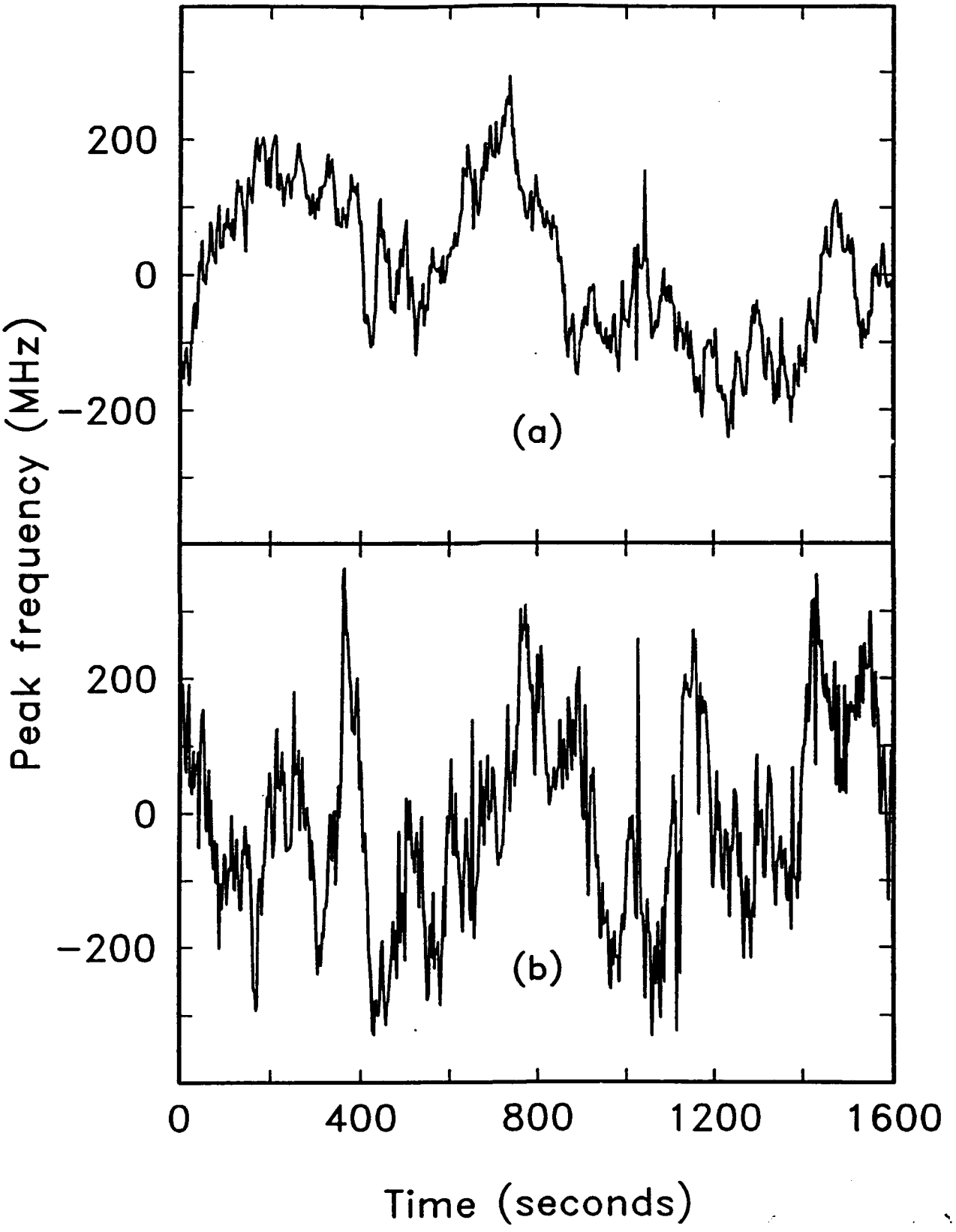
200
0
−200
(a)
200
0
−200
(b)
Peak frequency (MHz)
0
400
800
1200
1600
Time (seconds)

FIG. 13

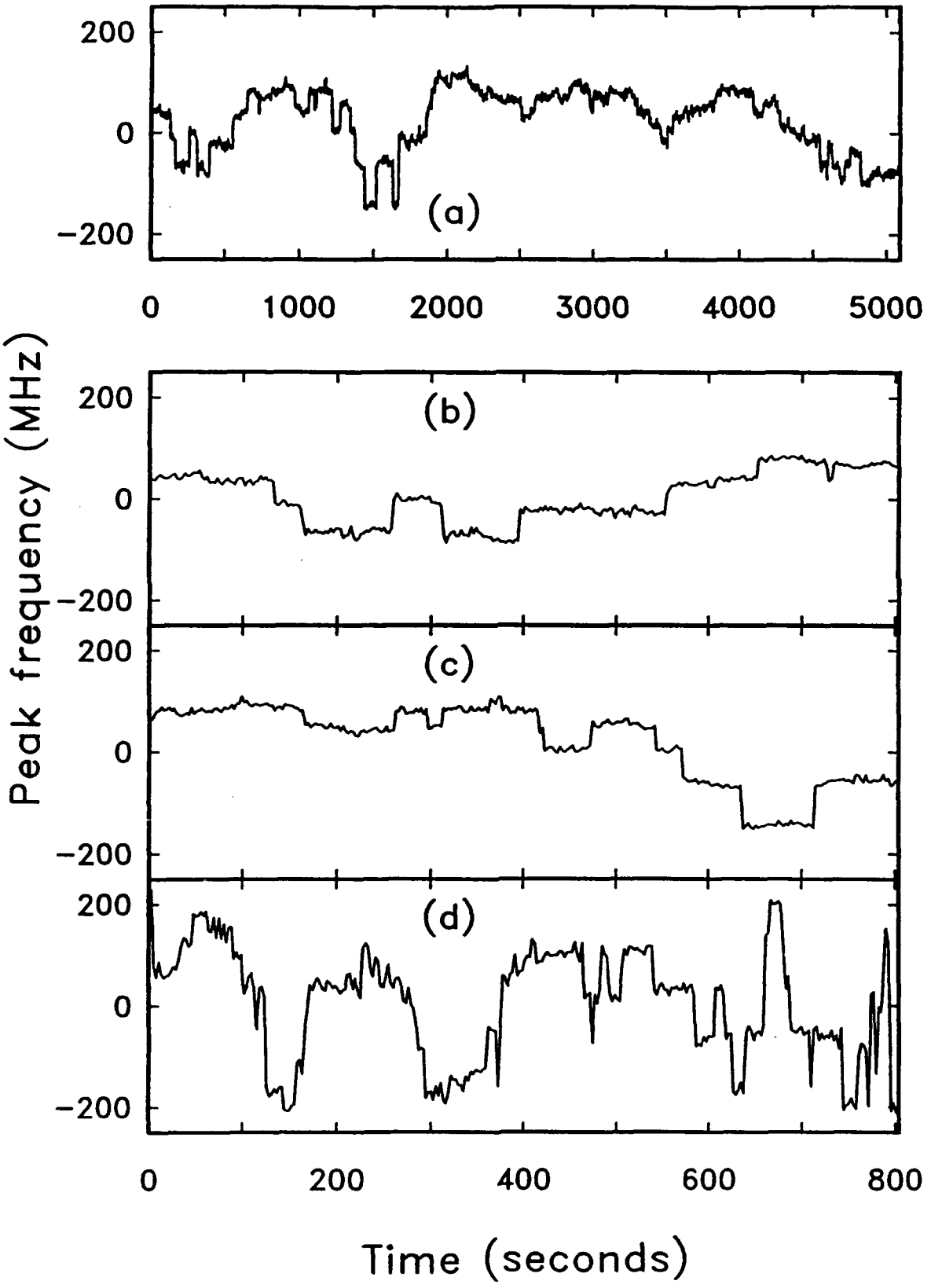
200
0
−200
(a)
0
1000
2000
3000
4000
5000
Peak frequency (MHz)
200
0
−200
(b)
200
0
−200
(c)
200
0
−200
(d)
0
200
400
600
800
Time (seconds)

FIG. 14

1. Office of Naval Research (2)
   Chemistry Division, Code 1113
   800 N. Quincy Street
   Arlington, VA 22217-5000

2. Defense Technical Information Center (2)
   Building 5, Cameron Station
   Alexandria, VA 22314

3. Commanding Officer
   Naval Weapons Support Center
   Attn: Dr. Bernard E. Douda
   Crane, Indiana 47522-5050

4. Dr. Richard W. Drisko
   Naval Civil Engineering Laboratory
   Code L52
   Port Hueneme, CA 93043

5. David Taylor Research Center
   Dr. Eugene C. Fischer
   Annapolis, MD 21402-5067

6. Dr. James Murday
   Chemistry Division, Code 6100
   Naval Research Laboratory
   Washington, D. C. 20375-5000

7. Dr. Robert Green, Director
   Chemistry Division (Code 385)
   Naval Weapons Center
   China Lake, CA 93555-6001

8. Chief of Naval Research
   Special Assistant for Marine Corps Matters
   Code 00MC
   800 North Quincy Street
   Arlington, VA 22217-5000

9. Dr. Bernadette Eichinger
   Naval Ship Systems Engineering Station
   Code 053
   Philadelphia Naval Base
   Philadelphia, PA 19112

10. Dr. Sachio Yamamoto
    Naval Ocean Systems Center
    Code 52
    San Diego, CA 92152-5000

11. Dr. Harold H. Singerman
    David Taylor Research Center
    Attn: Code 283
    Annapolis, MD 21402-5067